The importance of structural complexity in the localization of geothermal systems: a case study along the Vallès-Penedès Fault in the Catalan Coastal Ranges (NE Spain)

G. Mitjanas[a], J. J. Walsh[b], E. Roca[a], G. Alías[c], P. Queralt[a], J. Ledo[d], P. Piña-Varas[a]

[a] Departament de Dinàmica de la Terra i de l'Oceà, Universitat de Barcelona, C/ Martí i Franquès s/n, 08028, Barcelona, Spain.

[b] Fault Analysis Group and Irish Centre for Research in Applied Geosciences (iCRAG), UCD School of Earth Sciences, University College Dublin, Belfield, Dublin 4, Ireland.

[c] Departament de Mineralogia, Petrologia i Geologia Aplicada, Universitat de Barcelona, C/ Martí i Franqu`es s/n, 08028, Barcelona, Spain

[d] Departamento de Física de la Tierra y Astrofísica, Facultad de Física, Universidad Complutense de Madrid, Spain.

Corresponding author: Gemma Mitjanas (gmitjanas@ub.edu)

Abstract

The Vallès-Penedès Fault is a Neogene normal fault marked by the presence of two established geothermal systems at La Garriga-Samalús and Caldes de Montbuí within the Catalan Coastal Ranges of NE Spain. The analysis and collation of existing and new geological and geophysical datasets provide the basis for the development of an improved conceptual model for the presence and localization of hot geothermal fluid systems at relatively shallow depths (e.g., 60^0C at surface and 90^0C at 1 km). Geothermal flow is concentrated within Paleozoic granodiorites of the immediate footwall of the V-P Fault, host rocks that are susceptible to fault-related fracturing, and the generation of both extension and hybrid fracture systems in association with active fault displacements. Flow localization is enhanced further by the presence of fault-related structural complexities, with both systems marked by 300 m wide steps in the main fault trace. These are attributed to relay development and breaching characterizing host rocks by high fracture intensities and fault rock development on a fault that locally has a vertical displacement of over 1.5 km. Accentuated fracturing and deformation are consistent with strain localization predicted by existing models for the development of fault zones along normal faults. The plumbing of the geothermal systems is attributed to up-fault flow in combination with lateral flow controlled by the intersection of the V-P fault with a low-angled Paleogene thrust defining the base of the host-rock granodiorites, with the geothermal systems localized at distil end of the thrust. Sustainable geothermal flow is attributed to groundwater flow circulation associated with seismic pumping and valving of warmer and deeper fluids, and the ingress of groundwater along faults and within fractured basement rocks.

Keywords

Method combination, geothermal exploration, geophysics, fault zones

1. Introduction

Faults have long been known to significantly influence on the migration of fluids within the crust, often acting as the principal conduits and traps for groundwater, hydrocarbon, and mineral flow systems (Sibson 1987, Faulkner et al. 2010, Micklethwaite et al. 2014, Walsh et al. 2018). Recent work has highlighted their importance in the formation of low-high enthalpy geothermal reservoirs (Bellanger et al., 2019; Duwiquet et al., 2021), providing the conduits and storage for hydrothermal fluids and playing a pivotal role in the emergence of sustainable flow circulation systems. Within otherwise relatively impermeable rock volumes, such as granites, basement rocks or massive limestones, faults often comprise zones of more permeable fault rocks bounded by highly fractured host rocks, together representing the essential flow components of multiple fault networks (Achtziger-Zupančič et al., 2017; Bellanger et al., 2019; Duan et al., 2017; Haines et al., 2016; Siebenaller et al., 2013; Süer et al., 2008). By contrast, within higher porosity-permeability host rocks, such as clastic sediments, fault rock can represent seals or baffles to across-fault flow (e.g. Fisher & Knipe 1998; Manzocchi et al. 2010; Yielding 2002), but can also act as pathways for along-fault flow (e.g. Rowe and Burley 1997; Selley et al. 2005; Walsh et al. 2018; Wibberley et al. 2008). This duality of flow behaviour, depending on host rock properties and flow direction, means that faults and fractures often exercise a major control on the plumbing of flow systems in the subsurface (Sibson 1987, 1998; Faulkner et al. 2010; Walsh et al. 2018).

Previous studies have highlighted how the complexities of fault zone structure arising from fault propagation and localization can often provide important pathways for fluid flow. The formation and evolution of major faults are associated with the nucleation and growth of fault segments during the deformation (Cartwright et al., 1996). The overlap and linkage of such fault segments is often marked by zones of accentuated deformation associated with the formation of relay ramps (Camanni et al., 2019; Cartwright et al., 1996; Childs et al., 1995; Fossen and Rotevatn, 2016; Mansfield and Cartwright, 2001; Peacock and Sanderson, 1994). Increases in faulting, fracturing and fault rock development adjacent to these fault zones (fault zones) can have a controlling influence on the migration of fluids, acting as a fluid conduit, barrier, or combined conduit-barrier system (Faulds and Hinz, 2015; Manzocchi et al., 2008; Rotevatn et al., 2009b, 2009a).

The general conceptual model for fault zones involves high-strain localizations of fault rock and slip surfaces, often referred to as the fault core, surrounded by fractures and faulting in a lower-strain damage zone (Faulkner et al., 2010; Passchier and Trouw, 2005). In practice, the distribution of damage is very heterogeneous, often reflecting the 3D segmentation and bifurcation of fault surfaces (Childs et al. 2009), and it is this heterogeneity of structure which localizes fluid flow. Fault zones comprise cataclastically deformed host rocks, including brecciated, indurated, and geochemically altered host rocks, unconsolidated clay-rich gouge zones and internal multiple slip surfaces (Anderson et al., 1983; Caine et al., 1996). This fault core is mainly characterized by lower porosity and permeability, and is generally considered to act as a flow barrier to across-fault flow (e.g., Manzocchi et al. 1999, 2010; Wibberley and Shimamoto, 2002), but can, at the same time, act as a conduit for along-fault flow (Sibson 2000; Walsh et al. 2018). The surrounding lower-strain damage zone can be very heterogenous in structure, comprising faults and fractures (including hybrid and extension structures) over a wide range of length scales, often generating high permeability conductive networks within otherwise low permeability host rocks (Faulkner et al., 2010).

Whilst fault zones have been extensively studied in geothermal exploration studies (Géraud et al., 2010; Loveless et al., 2014; Siler et al., 2018), previous work has less often investigated the significance of structural complexity for a geothermal system. For example, the geometry and nature of fault intersections, splays, relays, and associated damage-related fractures, are usually not considered in the context of flow localization and host-rock alteration. Nevertheless, earlier studies on West European Rift Systems have demonstrated that high thermal gradient locations along fault zones on normal faults are very prospective as high enthalpy geothermal targets (Bertrand et al., 2013; Duwiquet et al., 2019; Loveless et al., 2014; Rhén et al., 2007). In this paper, we describe the geometry, deformation and flow indicators (e.g., alteration patterns and vein infills), and investigate the relationship between key structural parameters and the localization of a geothermal system. The study is within the Catalan Coastal Ranges (CCR) and along the Vallès-Penedès Fault, a major crustal fault bounding the NW margin of the Vallès-Penedès Basin (Fig. 1). The NE end of this major basement fault has been established as the main locus for the hot fluids of the La Garriga, Samalús, and the Caldes de Montbui geothermal systems. Our study focusses on the La Garriga-Samalús geothermal system (Fig. 2), which has been the subject of several previous studies (Canals et al., 1989; Cardellach et al., 2002; Fernàndez and Banda, 1990, 1988; Mitjanas et al., 2021). We present a geological and structural characterization of the controlling structures of this geothermal system, utilising the geophysical data presented in Mitjanas et al. (2021). In addition, a 3D geothermal model is presented of the northeastern part of the Vallès basin, highlighting the pivotal role of structural complexity in the functioning of the geothermal system.

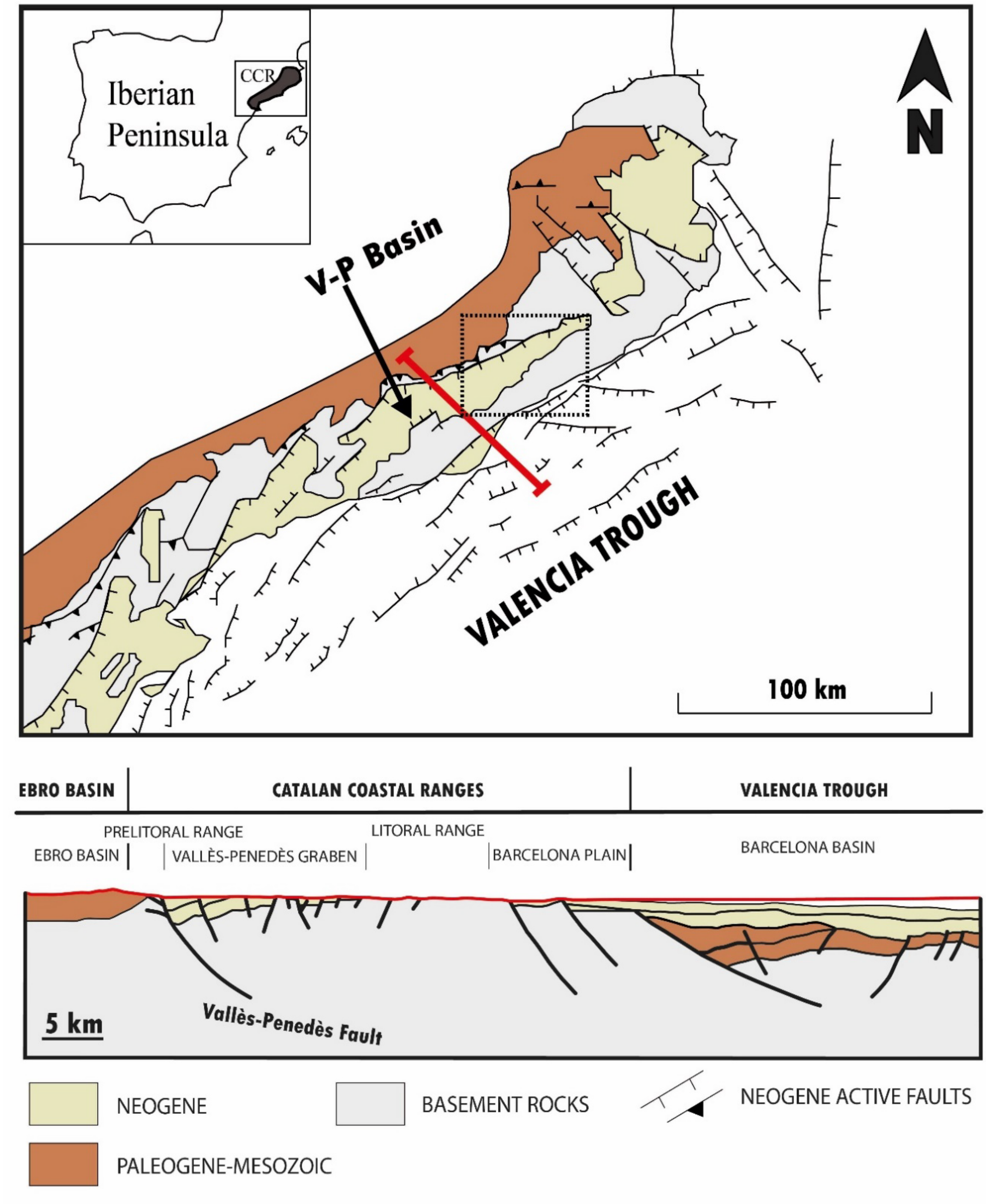

Figure 1. *(a) Structural map of the Valencia trough, showing the Catalan-Valencian domain (modified from Marti et al., 1992). This map highlights the orientation of the main NE-SW trending normal faults providing onshore Neogene basins (yellow), including the Vallès-Penedès (V-P) basin. Towards the west, the V-P fault bends into a NNE-SSW orientation, whereas towards the northeast, the fault dies out and is replaced by a NW-SE fault system which in turn transfers to another NW-SE trending normal fault system in the north. (b) Cross-section derived from interpreted seismic data (Roca et al. 1999) highlighting the rotated fault blocks and hangingwall syn-rift infill of the V-P Basin and the Barcelona Basin.*

2. Geological and geothermal setting

2.1. Vallès-Penedès Fault

The Vallès-Penedès (V-P) Fault, an ENE-trending major crustal normal fault more than 100 km in length, is located in the Catalan Coastal Ranges (CCR), in the NE of the Iberian Peninsula (Fig. 1). The CCR are the onshore southern extension of the Catalan margin, comprising the Prelitoral and Litoral ranges that are separated by the Vallès-Penedès half-graben basin. The V-P Fault, which limits the Prelitoral Range from the Vallès-Penedès Basin, has a cumulative displacement of up to 4 km, which developed from approximately Oligocene to Present times (Bartrina et al., 1992; Gaspar-Escribano et al., 2004; Roca et al., 1999a; Santanach et al., 2011). The present configuration of the CCR mainly arises from the late Oligocene-early Miocene opening of the Valencia Trough (Western Mediterranean) (Bartrina et al., 1992; Roca, 2001). This trough comprises several ENE- to NE-striking basement blocks bounded by 50 to 150 km-long normal faults (Gaspar-Escribano et al., 2004). These major normal faults dip towards the SE and define a system of major half-graben filled by Miocene deposits. Previous work suggests that some of these faults are long-lived structures, which, before their most recent Neogene activity, could have originally formed during the Mesozoic opening of the Tethys (Martín-Martín et al., 2021) and later accommodated contractional inversion during the Paleogene collision between Iberia and Eurasia (Fontboté et al., 1990; Roca et al., 1999b).

The V-P Fault separates a basin filled with Miocene sediments in the SE from an outcropping Variscan basement in the NW. The footwall basement forms a mountain range up to 1700 m high, referred to as the Prelitoral Range, which has been attributed to isostatic footwall uplift of 2 km during the Neogene activity of the V-P Fault (Gaspar-Escribano, 2003). The immediate footwall to the V-P Fault comprises a NNW-directed granodioritic Paleogene thrust sheet, which overthrusts a series of Cambro-Ordovician to Carboniferous metamorphic rocks. The Paleogene thrust sheet is a major reverse fault system with a component of sinistral horizontal displacement oblique to the direction of maximum shortening of the Pyrenean zone (Anadon et al., 1985; Gaspar-Escribano et al., 2004; Guimerá, 1984; Roca, 1996; Roca et al., 1999b). The footwall metamorphic series comprises slates, quartzites, and minor limestones (ICGC, 2006; IGME, 1974), and the post-Variscan intrusive unit comprising granodiorites intruded by E-W aplite, pegmatite and granitic porphyry dykes (ICGC, 2006). By contrast, the basin infill of the V-P Fault comprises conglomerates, arkosic sandstones, and mudstones, forming an alluvial fan sequence containing big boulders of the Prelitoral Range igneous and metamorphic rocks (ICGC, 2006, 2002; IGME, 1974) immediately adjacent to the V-P Fault. The precise thickness of the V-P Basin is not well established, as demonstrated by the differing thicknesses shown on previously published geological cross-sections (Fernàndez and Banda, 1990, 1988; Fontboté, 1954; IGME, 1977; Mitjanas et al., 2021; Roca, 1992).

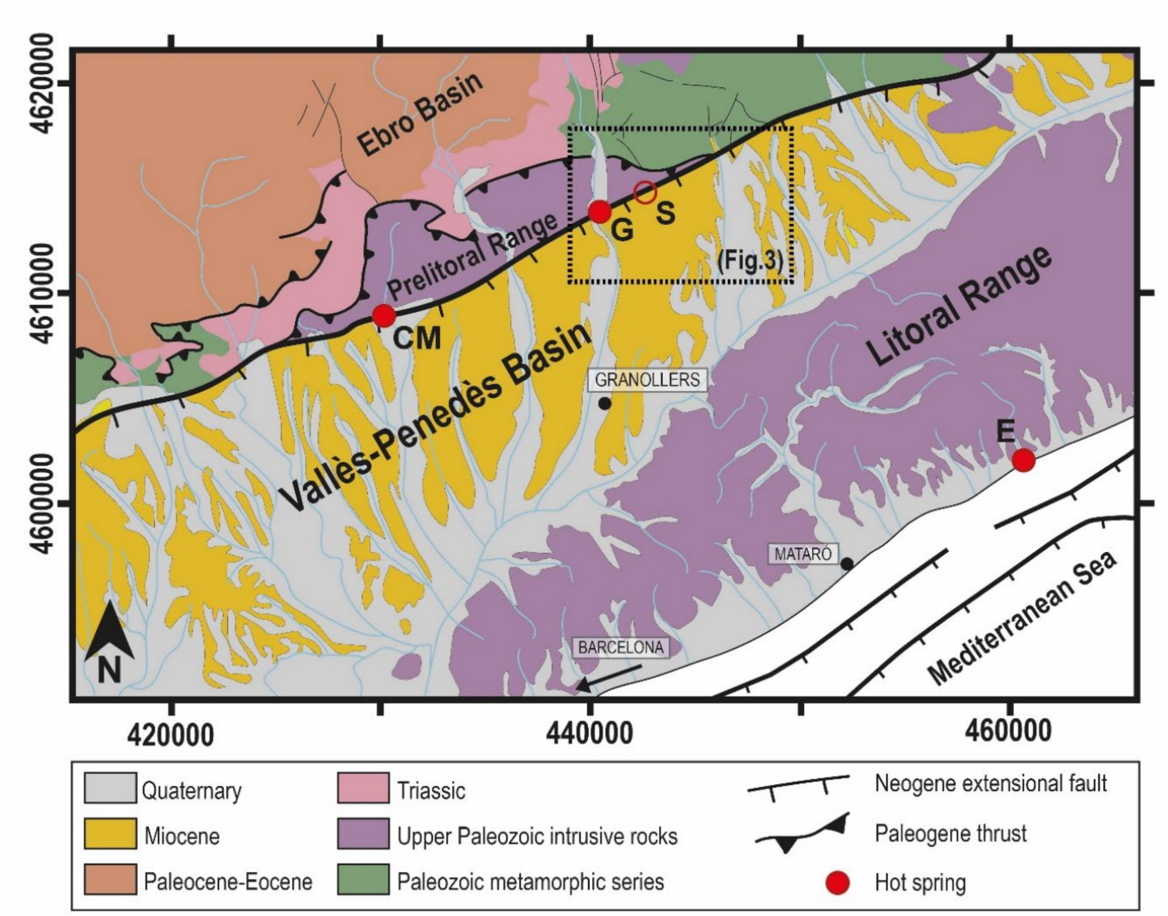

Figure 2*. Geological map (UTM coordinates) of the central to eastern part of the Catalan Coastal Ranges, highlighting the Vallès-Penedès Basin and its bounding southward-dipping Vallès-Penedès (V-P) fault. Normal faulting of Neogene age has generated a Miocene filled half-graben, which deepens and widens along-strike towards the west and gives way to the south to similar southward-dipping normal faults which bound the offshore Valencia Trough. Hot springs along the V-P Fault are located where the footwall rocks are Upper Palaeozoic granitic intrusives in the hangingwall of a southward dipping Paleogene thrust study area (red square; need to make sure the location box is the correct shape and location relative to next figure) and the location of the towns with thermal hot springs:* ***CM*** *- Caldes de Montbuí (70ºC);* ***G*** *- La Garriga (60ºC);* ***E*** *- Caldes d'Estrac (38ºC); and other indicators of thermal activity:* ***S*** *- Samalús (90ºC at 1000 m depth). The study area is indicated by the red outlined square (Modified from ICGC, 2002 and Martí et al., 1992).*

2.2. La Garriga-Samalús geothermal system

Two localities are marked by geothermal activity along the V-P Fault trace (Fig. 2): La Garriga-Samalús (G-S) and Caldes de Montbuí (CM). Both have similar structural configurations insofar as they are in the vicinity of the NE and SW branch points, respectively, between the NNW-directed Paleogene thrust and the V-P Fault (Fig. 1). They are, however, marked by different thermal waters, with the La Garriga water springs having sodium bicarbonate compositions and a surface temperature of ca 60ºC, and those of Caldes de Montbui having sodium chloride compositions with the temperature of ca 70ºC (IGME, 1986). Previous studies were mainly focused on the Caldes de Montbui hot spring, where the onset of the geothermal activity was dated as middle/late Miocene and the thermal waters are characterized by the mixing of hydrothermal fluids and meteoric waters, and the precipitation of pedogenic products along faults (Cantarero et al., 2014a, 2014b). Our study is focused in the G-S geothermal system where the structure is better known from geological and geophysical data collected in previous studies. Later we will consider aspects of both geothermal systems in an effort to define a unified model for their formation

The G-S geothermal system was previously studied during the 1980's, when the geological survey of Spain investigated the geothermal potential of Spain (IGME, 1982, 1984, 1986). At this time, six exploration boreholes S1 (IGME, 1982), S2-S5 (IGME, 1984), and S6 (IGME, 1986), were drilled in Samalús town, with the last one recording 90ºC at 1000 m depth. These boreholes were also complemented with some temperature profiles close to La Garriga town (Fig. 3). Later studies worked on the origin of the geothermal system and its broad conceptual framework (Canals et al., 1989; Cardellach et al., 2002; Fernàndez and Banda, 1990, 1988; Mitjanas et al., 2021). The derived geothermal model for the G-S system advocates convection through the uplifted footwall (Fernàndez and Banda, 1990), with a slow downward circulation of meteoric water until it reaches the V-P Fault, with later geophysical characterization interpreted to indicate completion of the cycle with fast ascending hot fluids migrating along the fault zone (Mitjanas et al., 2021).

3. Methods

In order to understand the La Garriga-Samalús geothermal system, this study integrates structural and petrographic analysis of the main fault and associated meso- and micro-scale faults/fractures, together with an evaluation of the hydraulic properties of the different units. Our work complements earlier geophysical data (Mitjanas et al., 2021), with the acquisition of a new magnetotelluric (MT) profile and additional ambient seismic noise (HVSR) sites (Fig. 3).

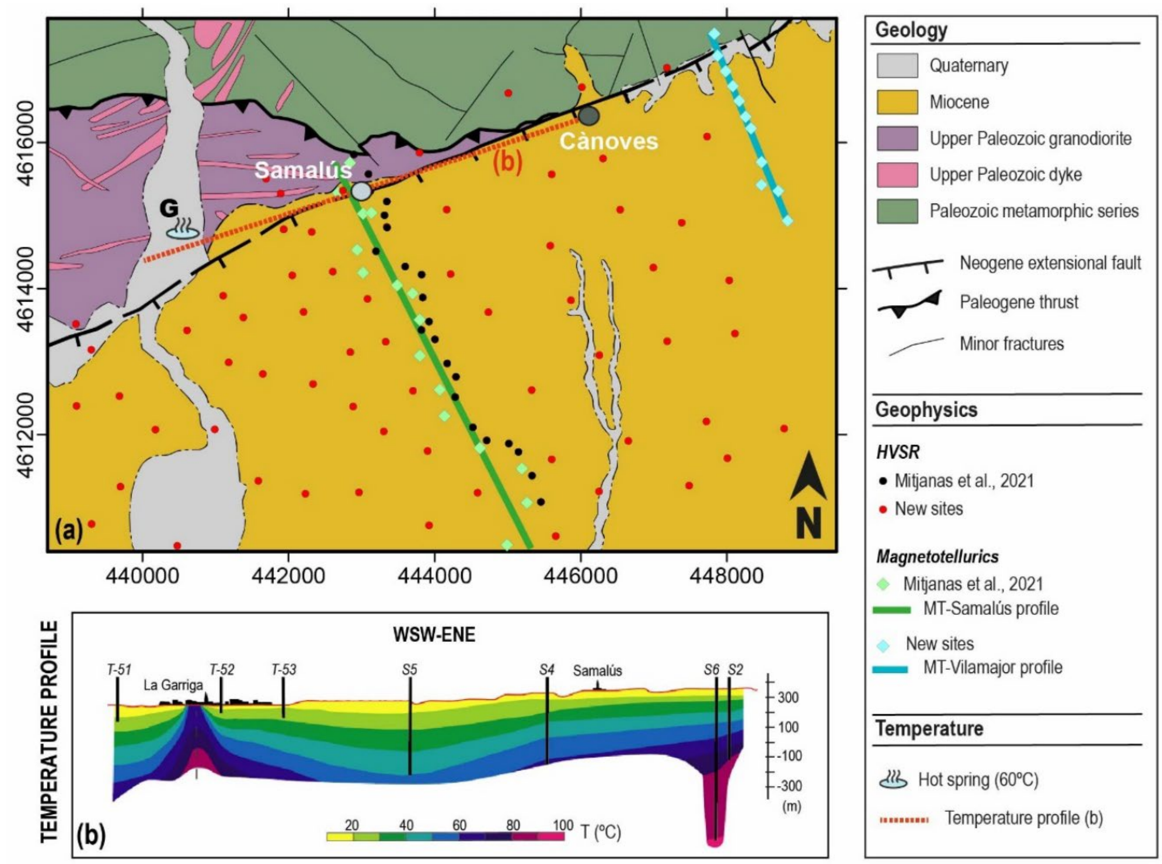

Figure 3. *(a) Geological map of the La Garriga-Cànoves region in which the location of the main towns and the temperature profile. The biggest town of the area, La Garriga (G), is the only with hot springs (60ºC), but the main exploration boreholes were made close to Samalús town. The location of the along-fault temperature variation cross-section shown in (b) is marked by red broken line. The sites for previous (Mitjanas et al., 2021) and newly acquired geophysical data (see legend for details) are shown, highlighting that this study provides HVSR data covering a 3D zone instead of just a profile and that an additional MT profile is now available outside of the granodioritic thrust sheet. (b) Temperature variations along cross-section parallel to the V-P fault (scale 1:1, see (a) for line location), derived from considerations of different temperature profiles (T) and borehole data (S) (Modified from IGME, 1984, 1986).*

3.1. H/V spectral ratio data

The horizontal-to-vertical spectral ratio (HVSR) technique applied to seismic ambient noise recordings, allows identification of large-impedance contrasts between sediments and underlying bedrock and is, therefore, an indicator of the bedrock hangingwall geometry (Bard, 1998, 1985; Nakamura, 1989). Our work includes more data sites than previous studies (Mitjanas et al., 2021), in order to provide better 3D definition of the La Garriga-Samalús footwall. The HVSR data acquisition and processing of 97 sites (Fig. 3) was carried out by the *Geophysical Techniques Department* of the *Catalan Cartographic and Geological Institute* (ICGC), following the same procedure described in Mitjanas et al. (2021). This methodology has already been applied in other Neogene basins near the Vallès basin (Benjumea et al., 2014, 2011; Gabàs et al., 2016; Macau et al., 2018; Mitjanas et al., 2021).

3.2. Magnetotelluric data

This study presents a new across-fault magnetotelluric profile (MT-Vilamajor) comprising 11 sites along an NNE-SSE profile of approximately 3 km length, from the footwall Prelitoral range into the hangingwall Vallès-Penedès basin sediments (Fig. 3). This MT profile is located to the east of Canovas town, where the granodiorite thrust sheet no longer outcrops, and to that extent, it complements an earlier published profile from Samalús town (MT-Samalús) spatially associated with the granodiorite-hosted geothermal system (Figs. 3 & 5; Mitjanas et al., 2021). The acquisition and processing procedure for this new MT profile is the same as described in Mitjanas et al. (2021). The calculated apparent resistivity and phase curves for the stations used in the modeling process can be accessed in the ***Supplementary Material (S.1)***.

3.3. Geological fieldwork

The geological fieldwork has been designed to improve the geological map of the area and, in particular, define the fault trace geometry of both the V-P Fault and the Paleogene thrust. The V-P fault trace, a critical determinant of the geometry and the potential plumbing of the system, has been defined from mapping the distribution of hangingwall Miocene sediments and footwall granites, on the one hand, and from across-fault terrain changes particularly those reflected in deflections of river systems, on the other. The locus of faulting has also been investigated from quantitative fracture analysis of footwall Variscan granodiorites immediately adjacent to the V-P Fault. Fracture geometry (dip and strike), and where possible fracture aperture, were measured for each fracture, with the spatial distribution of fractures analyzed using the linear scanline sampling method (Priest, 1993; Priest and Hudson, 1981; Schön, 2015; Watkins et al., 2015). This method permits the recording and analysis of a wide range of fracture attributes, though care needs to be taken about potential susceptibility to orientation bias when variably orientated fractures are sampled in a single scanline (Park and West, 2002). This methodology was applied to 50 footwall outcrops, providing an adequate means of investigating the spatial variations of fractures and of quantifying fracture density as a function of proximity to the V-P Fault trace: for the latter, distance against fracture density was estimated using the Natural Neighbour gridding method within *Surfer*® software (Golden Software LLC, 2016).

3.4. Petrographic characterization

Detailed petrographic analysis of secondary minerals and deformation textures has been performed on thin sections from outcrop and borehole samples to define the nature of deformation and fluid circulation within the damage zone of host rocks and the footwall granites, in particular. Our characterization of rock microstructure and the main mineral associations follows the procedure of Bertrand (2017) & Velde and Meunier (2008) on the following minerals to provide constraints on a variety of processes:

- Plagioclase and K-feldspars, to verify the alteration to clay minerals.
- Biotite, to investigate deformation and chlorite retrogression.
- Quartz, to identify micro-fractures, crystal deformation (e.g. undulate extinctions) and sub-grain recrystallization.

3.5. Structure-from-motion photogrammetry

Structure-from-motion photogrammetry (SfM) (Betlem et al., 2020) has been used to analyze fractures within 5 borehole core samples, in terms of their 3D nature and geometry, prior to thin section studies and further analysis. SfM processing was performed from digital images acquired using a remote-controlled system camera *Lumix G7* coupled with a *14-42 mm Lumix* lens, and following the workflow illustrated in the ***Supplementary material (S.2)***. The resulting point cloud for fractures has been analyzed using the open-source software *CloudCompare* (“CloudCompare [GPL software],” 2021).

3.6. Porosity measurements

Twelve samples from outcrops and the S1 borehole (IGME, 1982) have been analyzed in order to get porosity values of the granodioritic unit and the metamorphic Paleozoic unit. In order to get the porosity values, we used the geometry, the density (using a helium pycnometer), and the dry and wet mass of the sample, which details of the procedure are outlined in the ***Supplementary material (S.3)***.

The analysis of the selected samples was conducted in the *Institute of Geophysics and Geoinformatics* of the *Technical University of Bergakademie Freiberg* (Germany).

4. Results

4.1. V-P Fault geometry

The map geometry of fault traces is an important means of defining the location of structural complexities along normal faults. Various constraints are available for the study area, providing high-resolution areal definition of the fault trace geometry.

H/V spectral ratio data suggest a left-hand hangingwall bend in the vicinity of the La Garriga town, as defined by hangingwall sediment thicknesses of < 100 m (Fig. 4) approaching the surface trace of the sediment to basement contact. This bend is consistent with geological maps indicating a similar left-hand footwall bend or step bounding thin (< 100 m) Miocene sediments and footwall granite exposures (Fig. 3). Taken together, these bends suggest the presence a fault-bounded lens straddling what is mapped as the principal fault trace.

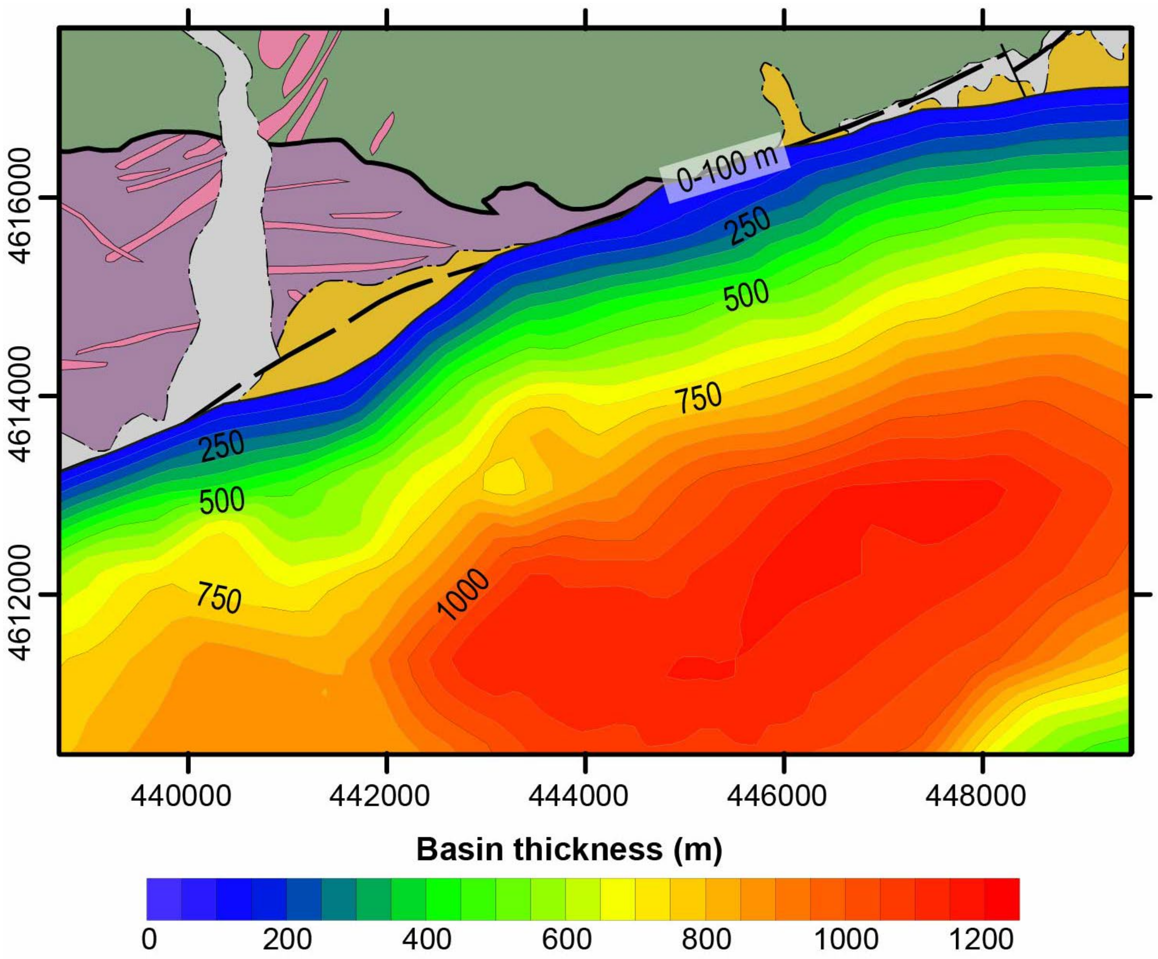

Figure 4. *Sediment thickness along the region of study, between La Garriga and Cànoves towns, derived from the horizontal-to-vertical (H/V) spectral ratio. The first contour (0-100 m) is set as a range since the accuracy of the final extrapolation from the measurement points does not allow to obtain an accurate limit this close to the topographic surface. Its thickness is up to a maximum of 1200 m towards the centre of the basin (SE), and the intersection of the presented surface and the topography seems to represent the V-P fault trace.*

This lenticular configuration is also consistent with terrain changes reflected in the trajectories of rivers cutting across the fault (Fig. 5), with single sharp deflections of rivers aligning with the approximately straight fault trace and with multiple deflections associated with the hangingwall and footwall bends enclosing an apparent lens in La Garriga town. Across the fault, the main river systems are approximately N-S or NNW-trending within the footwall of, and at a high angle to, the V-P Fault. However, they gradually turn towards more NNE-trending trajectories further to the south within the hangingwall basin fill (Fig. 2), particularly on regional scales as the southern footwall basement block is approached.

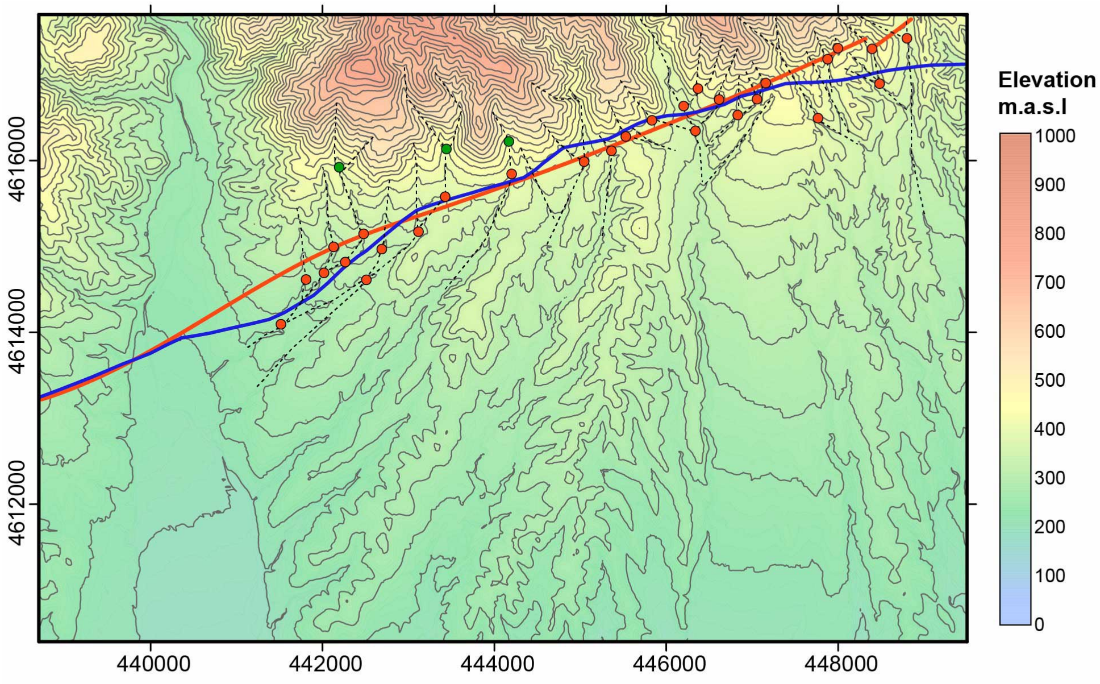

Figure 5. *Location of the main streams, rivers and ravines of the drainage network between La Garriga an Cànoves towns, together with the sediment-footwall map contact. Red points indicate inflexion points in the river course orientation.*

The resistivity models for two cross-sections across the V-P Fault (Fig. 6) are consistent with the mapped locations of the fault trace (Fig. 7), but they also provide excellent constraints on the deep geometry of the V-P Fault zone and Miocene basin. On both cross-sections, the footwall basement rocks of the V-P Fault have very high resistivities (> ca 3000 Ωm) and bound fault zones up to ca 1km wide comprising lower resistivity rocks (< ca 300 Ωm) extending to depths of greater than ca 2 km below sea level. Within the hangingwall of the V-P Fault, near-surface Miocene sediments define a heterogeneous geo-electric unit characterized by resistivity values between 1 and 200 Ωm. This syn-kinematic Miocene unit increases to ca 1 km thick within about 3 km of the V-P Fault and towards the centre of the Neogene basin (Figs. 4 & 6), a change which could be accommodated by successive synthetic normal faults given the resolution of the available data.

Both MT cross-sections suggest that the footwall fault is steeply dipping (70º) and approximately planar, but with slight shallowing (to 60º) on the MT-Samalús profile. The most significant departure from planarity is, however, the hangingwall side of the fault zone on the MT-Samalús profile, which dips at closer to ca 45º. This shallowing is considered to be a local effect because conventional seismic suggests that a shallow dipping listric geometry is only developed at greater depths of between 5-10 km (Gaspar-Escribano et al., 2004; Roca et al., 1999). Slightly shallower fault dips could instead be tentatively attributed to the eastward plunging of the La Garriga left-hand bend or perhaps the presence of synthetic normal faults not easily observed beneath the Miocene syn-rift sediments (Figs. 4 & 6). The potential for synthetic faults within a few kilometers of the V-P Fault is supported by stepping off the imaged Miocene unit, with the extensive development of mapped river terrace deposits perhaps coinciding with the main fault zone of the eastern cross-section. In that sense, the mapped trace of the V-P Fault is simply the footwall-bounding structure of the fault zone (Fig. 7), with the potential for additional synthetics within a few kilometers wide zone, which accommodates the syn-rift thickening suggested by H/V spectral ratio data.

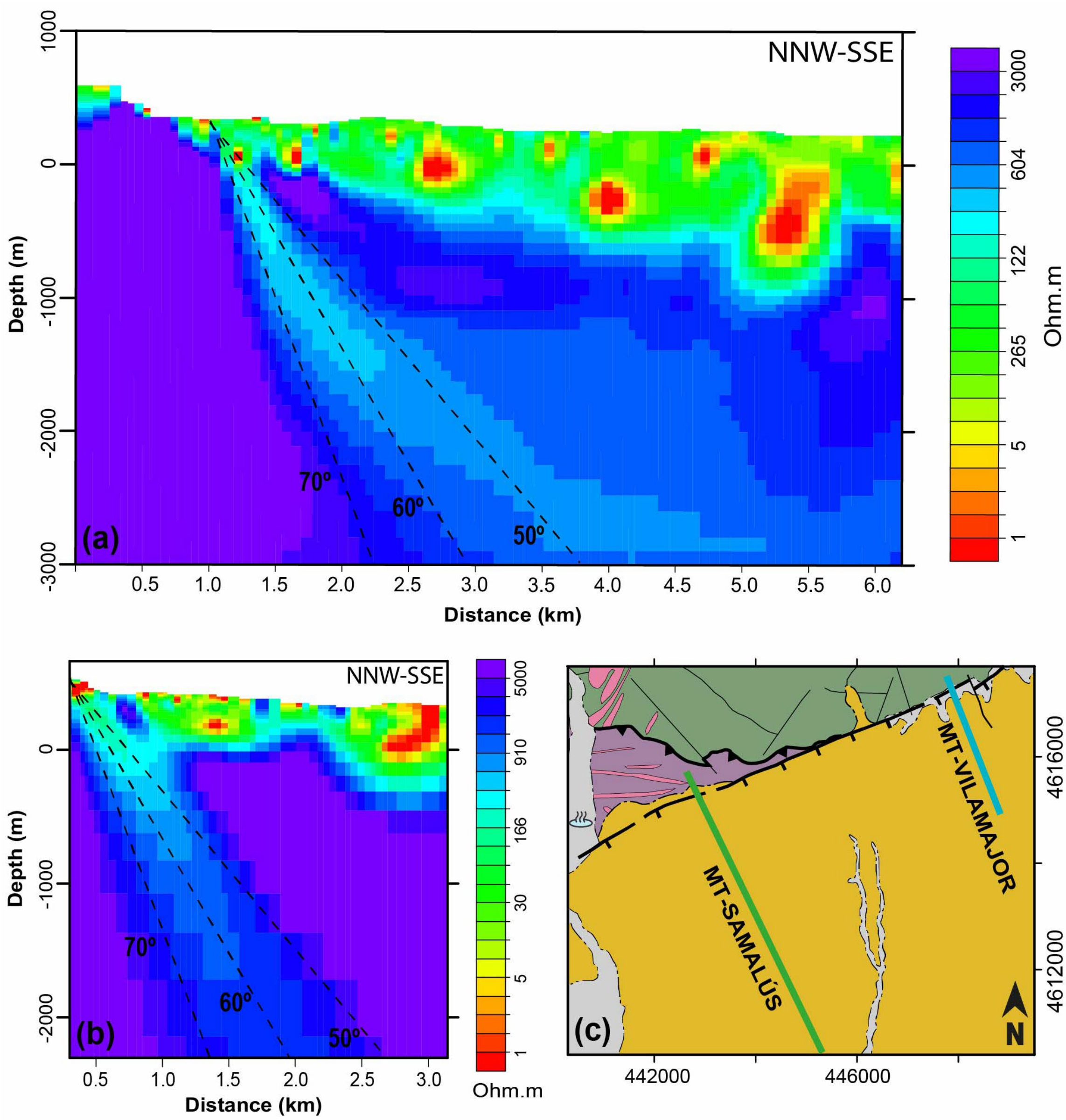

Figure 6. *Resistivity models for sections across the V-P fault showing along strike changes in the fault zone structure. (a) Western section indicating that the bounding fault has steep-moderate dips (70^0-50^0) towards the south, perhaps consistent with widening and shallowing in the west at the boundary to the fault bend at La Garriga. (b) Eastern section suggesting a steeper dipping fault zone (ca 70^0) which could be as wide as 500-750m.*

Resistivity modelling also provides some indication of the displacement on the V-P Fault. Previous work has suggested a vertical displacement of ca 4 km based on a conventional seismic line that transects the fault about 30-40 km to the west of La Garriga (Roca et al. 1999). Within the study area, Miocene syn-rift sediments are no greater than ca 1.25 km thick, a scenario which is attributed to an eastward decrease in displacement along the fault, with previous work indicating a fault tip and the end of the V-P hangingwall basin a further 25 km to the east (Fig. 1). Regional maps support the discontinuous nature of the V-P Fault and its hangingwall basin, with an overall mapped length of ca 120 km and a maximum displacement of 5 km (accounting for fault dip), scaling properties which are consistent with previously published normal fault databases (e.g., Nicol et al. 2020).

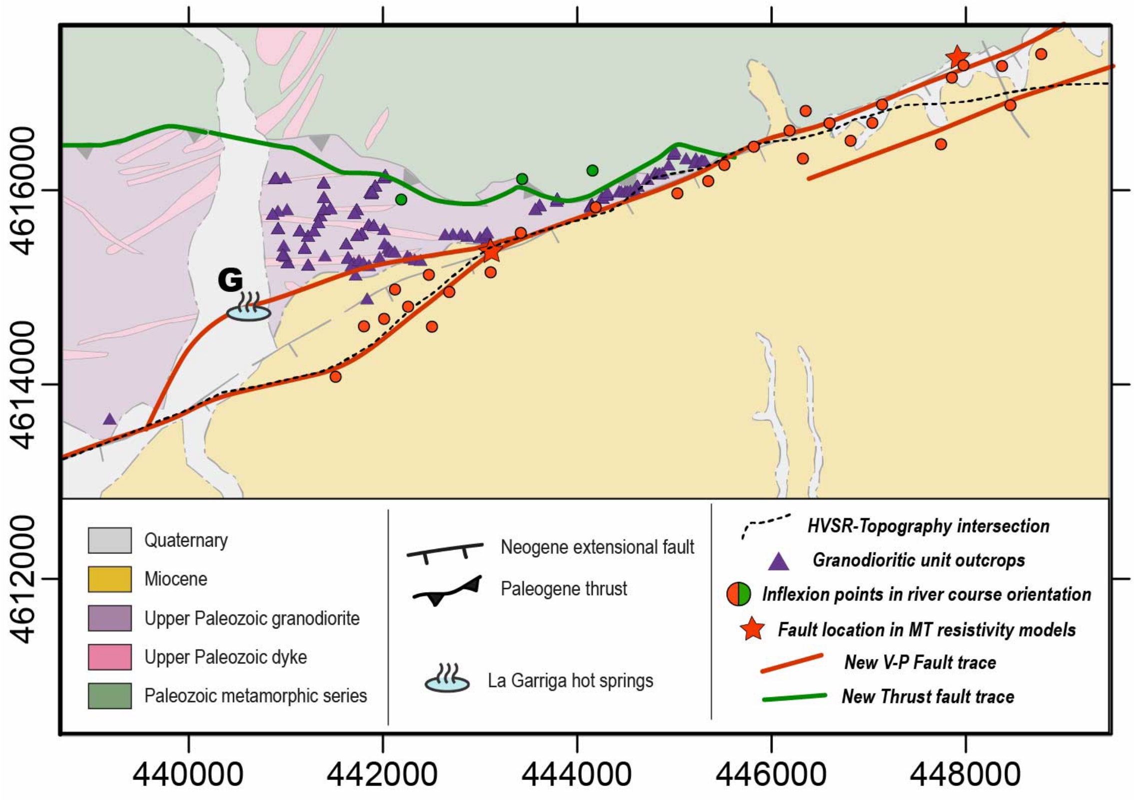

Figure 7. *Map showing constraints on the fault trace geometry of the V-P fault relative to earlier geological map (modified from ICGC, 2016). Evidence is derived from the following data: (i) the HVSR-Topography intersection line (green line; see also Fig. 4), (ii) the disposition of granodiorite outcrops, (iii) river inflection points (see Fig. 5), (iv) fault locations on MT resistivity models. The La Garriga river valley has occasionally been interpreted to contain a N-S fault of unknown origin, though its existence is not supported by any offsets of the V-F or the footwall Paleogene thrust. A new interpretation of the main V-P fault zone envisages a fault lens arising from the breaching of a left-stepping relay.*

4.2. Paleogene Prelitoral Thrust Geometry

The upper Paleozoic granodiorites within the footwall of the V-P Fault are contained in a thrust sheet overlying variably deformed Paleozoic metamorphic rocks. These units together are geographically referred to as the Prelitoral Range. At the surface, the thrust defines a broad bow-and-arrow geometry indicating an ENE-striking and SSE-dipping surface consistent with the characteristic

NNW-directed Paleogene shortening. The fault trace geometry of the thrust is locally irregular, indicating a shallow-moderate dipping surface (ca 15º and 50º) compared to the steeply dipping V-P fault. Although the available geophysical data do not permit 3D definition of the Prelitoral Thrust, previous exploration boreholes located in Samalús town, which extend to depths of up to ca 1 km (e.g. S6 borehole; IGME, 1986), do not cross the granodiorite-metamorphic contact, therefore suggesting prevailing thrust dips of ca 45º or greater. Such moderate fault dips provide some support for the notion that the thrust may have been derived from inversion of pre-existing normal faults along the site of the V-P Fault but they could also derive from associated footwall drag or minor synthetic fault displacements during Neogene extensional faulting. Whatever its precise geometry, the basic configuration of the thrust surface suggests a southward dipping thrust with the branch line between thrust and normal fault plunging towards the west in the La Garriga-Samalús study area and towards the east in the Caldes de Montbuí area. This geometrical arrangement is considered to be of first order significance for the geothermal system's plumbing, an issue which is considered later.

4.3. Deformation features of the thrust sheet unit

The deformation of the granodiorite rocks of the Paleogene thrust sheet unit has been characterized in terms of its fault rock development, fracture types, fracture intensity, and porosities. The host rock has been defined using the essential minerals of a granodiorite, quartz (25%), potassic feldspar (20%), plagioclase (40%), biotite (10%), and lesser proportions of accessory minerals (+5%). These host rocks are always affected by fracturing and alteration, which often show a sympathetic relationship and are spatially linked to the V-P Fault and, to a lesser extent, the Paleogene thrust.

4.3.1. Deformation of host rock granodiorites

The granodiorite host rocks are always highly fractured within the Paleogene thrust sheet. Background fracture densities are generally less than 0.1/meter on sample lines across the fracture system, with the average fracture network occupying up to 20% of the rock volume. These rocks show moderate degrees of replacement of orthoclase and plagioclase by kaolinite and sericite, with some deformation, kinking, and chlorite retrogression of biotite and the localized presentation of calcite (Fig. 8). Fracture networks normally comprise two preferred fracture orientations, with the development of more anastomosing systems with an increase in strain and fracture intensity. Fracture apertures visible at outcrop vary from 0.05 to 2 mm, and in some cases, they are infilled by calcite and iron oxides (i.e., Fig. 8B).

Approaching the V-P Fault plane, the granodiorite host rocks can become harder and more compact, increasing the difficulty of sampling. Petrographic analysis indicates a high degree of particle crushing contained within an aphanitic matrix enriched in quartz and calcite cement that is heterogeneously distributed but rarely represents more than 50% by volume. This protocataclasite comprises rounded-angular clasts (Fig. 8C), with cataclasis and straining of quartz and feldspar grains, and moderate to total alteration of feldspars. This development of protoclasite constitutes a fault core comprising up to ca 10 m thick of recrystallized and slickensided fault rock that appears in borehole cores to be hard, impermeable, and devoid of fractures. This fault rock is, in turn, bounded by a fault damage zone of high-intensity fracturing of the granodiorites that reaches ca 300 m beyond the fault surface.

Deformation adjacent to the Prelitoral thrust plane is more difficult to characterize however, it appears to be marked by the development of up to 4 m of incohesive impermeable gouge mainly derived from Ordovician slates in its footwall, a type of fault rock that has been previously identified in other parts of the CCR (i. e., Ribes Blaves fault gouge (Marcén et al., 2018)). Deformation of the footwall of the thrust is marked by ca 25 meters of fractured metamorphic unit below the main fault gouge, but the fracturing of the overlying hangingwall granodiorites unit is more pervasive (ca 50m) and intense.

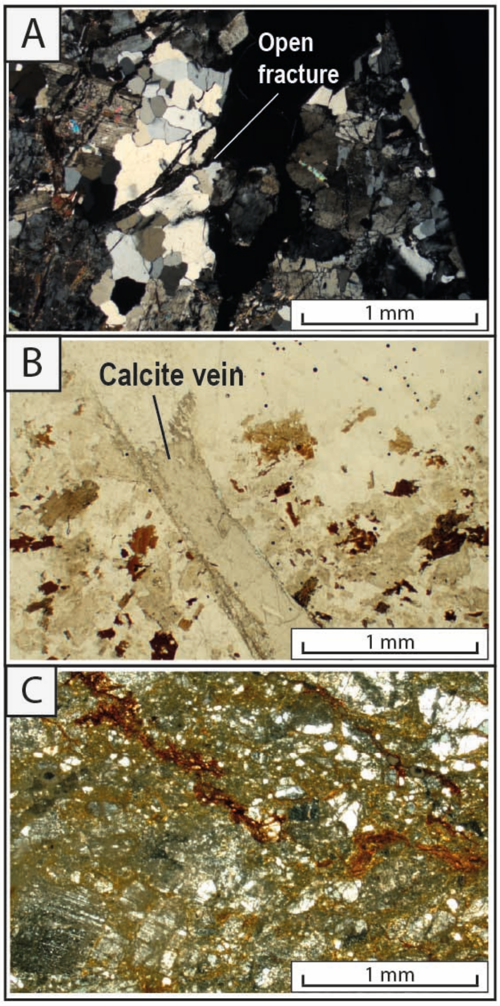

Figure 8. *A) Fractured granodiorite with open fractures. Sample shows undulant extinction, biotite deformation and sub-grain recrystallization (XP). B) Granodiorite with carbonate vein (PP). C) Protocataclasite and highly fractured rock in which it is possible to identify an associated matrix (XP).*

4.3.2. Fracture systems within granodiorites

Fracture characterization within the host rock granodiorites has resulted in the identification of 6 sets of outcrop-scale fractures with the characteristics outlined in Table 1 and Fig. 9. Moreover, the main orientations of fractures identified in boreholes point clouds (Fig. 10) match with those sets of fractures defined in the outcrops, with the most common fractures being F_A, followed by N-S steep (F_B) and shallow dipping (F_c) fractures. Although it has not been possible to determine the orientation of all of the borehole samples, together they permit fracture characterization without weathering and an assessment of the fracture apertures (2-4 cm) which can be both open and connected.

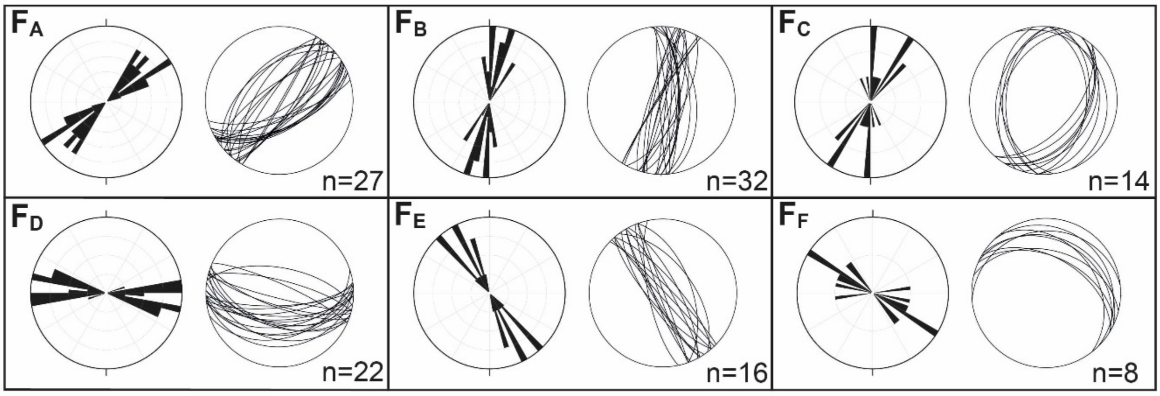

Figure 9. *Lower-hemisphere Schmidt stereonet and rose diagrams of the measured fractures grouped in the 6 fracture families distinguished in the granodiorite of the Prelitoral thrust sheet.*

From the few observable outcrops crosscutting relationships, the following chronology of the distinguished fracture families has been established: 1) F_F; 2) F_E; 3) F_D; 4) F_B and F_C; and, finally, 5) the F_A. Since no radiometric ages of veins are available in this area, there are no direct chronological constraints on the timing of fracture sets. Despite that shortcoming, potential geometric correlations (e.g., dip and strike) can be made between fracture sets and the main tectonic events, the relative timing of which is better defined from previous studies. On geometrical and kinematic grounds, we consider the F_D, F_E, and F_F fractures as the oldest fracture sets developed during the later stages of magma cooling related to the Variscan Orogeny. Cooling joints in magmatic intrusions are very frequently displaying a characteristic pattern of vertical (F_E) and sub-horizontal fractures (F_F) (Cloos, 1922; Mattsson et al., 2020; Price and Cosgrove, 1989). F_D fractures have the same orientation as the E-W dyke swarm of aplites and pegmatites, suggesting that they may be cooling fractures following the ascent of late granitic intrusions. Whilst fractures related to Mesozoic deformation have previously been described in the western part of the Vallès basin (Cantarero et al., 2014), our study has not identified fractures attributable to this deformation. Instead, the temporal activity of F_B and F_C fracture sets is unclear but is tentatively attributed to the Tertiary. Previous work has suggested that the Alpine orogeny (Eocene-Oligocene) was marked by NW-SE and N-S compression during earlier phases to be replaced by later NE-SW (Guimerá and Santanach, 1978). The main expression of Alpine deformation in the study area is the Prelitoral Thrust, with minor fractures previously considered to be strike-slip fractures with NW-SE and E-W orientations

(Guimerá, 1984; Guimerá and Santanach, 1978), perhaps involving the reactivation of the previously fracture sets. Instead F_B, and F_C fracture sets are attributed to post-Alpine deformation as follows. The V-P Fault is the main expression of the Neogene rifting event (Bartrina et al., 1992; Cabrera and Calvet, 1996; Fontboté et al., 1990; Roca and Guimerà, 1992), with the F_A fracture set striking and dipping in the same orientation, with greater intensities adjacent to the fault trace, but with borehole samples indicating dip-slip slickenlines. Whilst cross-cutting relationship suggests that F_B and F_C are cross-cut by F_A, they are spatially distributed across the study but are densely localized close to the V-P Fault trace at La Garriga town and the branch point between the Prelitoral thrust and the V-P Fault. In the circumstances, their origin is tentatively attributed to localized deformation that is accentuated adjacent to structural complexities associated with the V-P Fault, including branch points and the breached relays.

ID	Strike	Dip	Aperture	Infillings
F_A	NE-SW	50º – 88º	1 mm – 4 cm	Mostly unfilled (not-determined)
F_B	N-S to NNE-SSW	66º – 90º	4 mm – 2 cm	Unfilled
F_C	N-S	16º – 55º	0 mm – 2 mm	Filled (kaolin)
F_D	E-W	28º – 84º	2 mm – 1 cm	Filled (not-determined)
F_E	NW-SE to NNW-SSE	57º – 89º	1 mm – 3 mm	Mostly unfilled (carbonated)
F_F	WNW-ESE	73º – 86º	0 mm – 2 mm	Unfilled

Table 1. Fracture sets identified in the granodiorite of the Prelitoral thrust sheet.

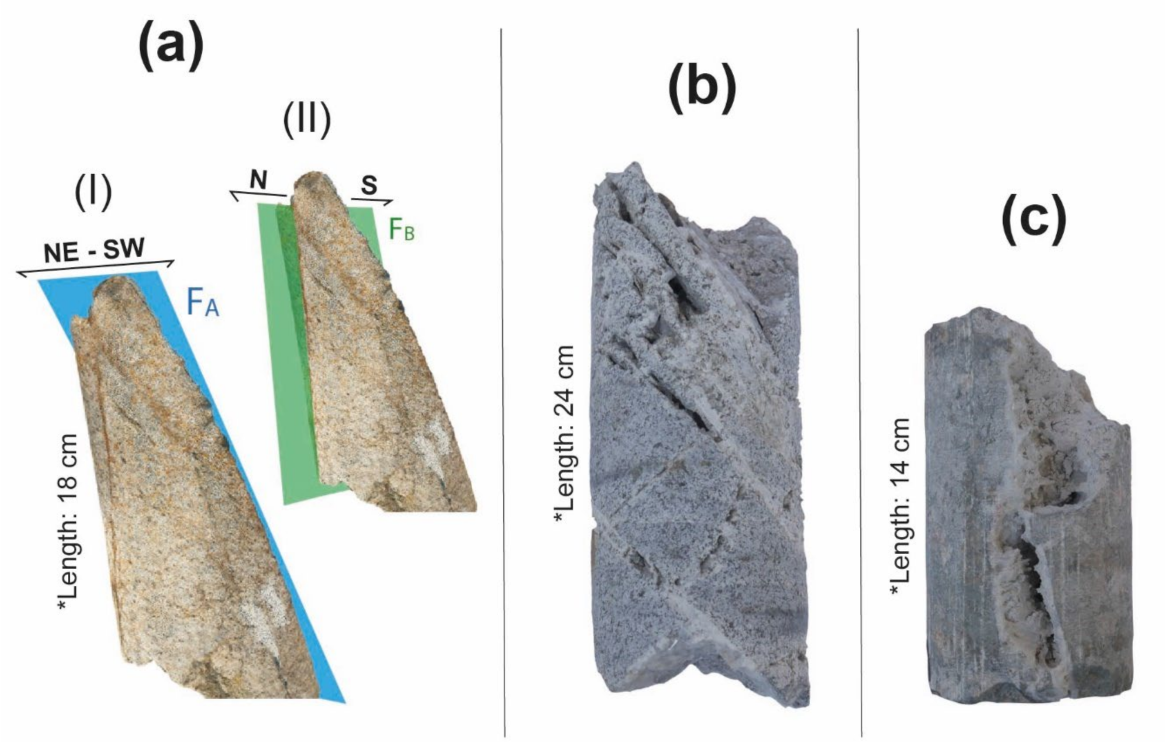

Figure 10. *S1 borehole core samples. (a) Oriented sample used to relate the family sets described in outcrops with the deep fractures. (b & c) Not oriented samples of a granodiorite (left) and a leucogranite (right) with open fractures partially filled by hydrothermal carbonated precipitates.*

4.3.3. Fracture intensities

Quantitative characterisation of the V-P damage zone has been performed by measuring fracture density from nearly 50 outcrops, each providing average sample line lengths of ca 5 m. The resulting intensity map (Fig. 11) highlights an increase in fracture intensity towards the V-P Fault and, to a lesser extent, the Prelitoral Thrust. Average fracture intensities can reach values as high as 0.5/m approaching the V-P Fault, though the heterogeneous nature of fracture spatial distributions is typical at all scales. High intensities are typical of outcrops within ca 200 m of the V-P Fault, an observation which is consistent with open and connected fractures seen in both outcrops and boreholes. Taken together the fracture intensity data support the notion of a damage zone marked by enhanced fracturing within the immediate footwall of the V-P Fault.

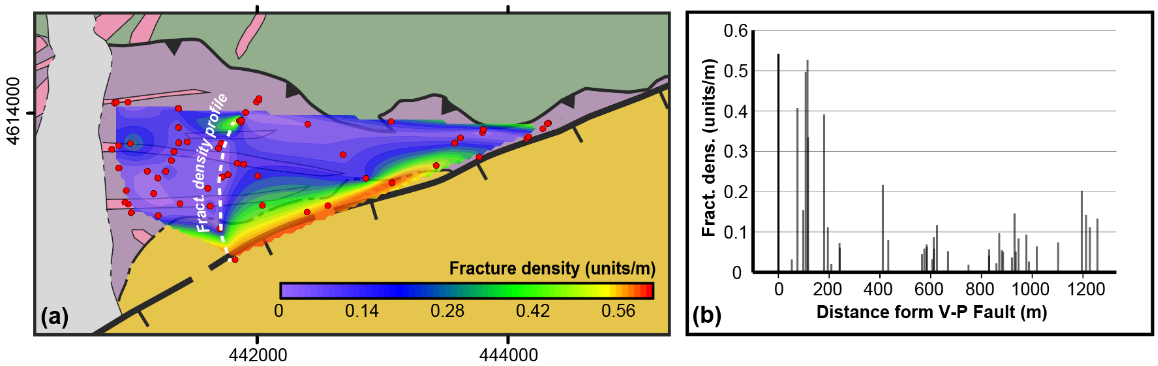

Figure 11. *Fracture intensity map and graph for the granodiorites within the footwall of the V-P fault. (a) Map with contours of the average fracture intensity (/m) for different outcrops (red dots). (b) Graph presents the average fracture density per meter sampled for individual outcrops in (a) projected onto a sample line (white broken line) extending from the V-P fault to the Prelitoral thrust; each outcrop is marked by a vertical line denoting the average fracture intensity.*

5. Porosity characteristics and distribution

Porosity measurements have been defined for granodiorite, dyke and metamorphic rocks sampled from outcrops, and for granodiorites sampled from the S1 borehole adjacent to Samalús. Outcrop samples for the granodiorite and dyke samples have porosities of between 5% and 30%, with the finer grained dykes providing lower porosity samples (5-15%). Petrographic analysis of these samples indicates the importance on weathering with varying degrees of alteration likely to dominate the associated porosity measurements, which are relatively high for conventional granites. By contrast borehole-derived porosities are both lower (1-10%) and are usually marked by fracture-related porosity as opposed to secondary porosities arising from weathering, values which are therefore considered to be more representative of the deeper subsurface (see below). Samples of metamorphic rocks underlying the Paleogene thrust have much lower and more consistent porosities of ca 5%, values we attribute to fracturing considering the otherwise unweathered nature of those host rocks compared to the overlying granodiorites. Existing constraints are relatively sparse at present but they do not suggest a direct relationship between the sample porosity and proximity to the V-P fault plane, a feature we attribute to the heterogeneous nature of deformation and alteration.

6. *Estimation of groundwater flow parameters*

Whilst porosity measurements for the host-rock granodiorite within the sub-surface suggest that weathering can generate porosity within the host-rock granodiorites, examination of borehole data indicates that deep sub-surface processes are dominated by fracture-controlled porosity arising from vuggy and high-intensity arrays of fractures and by associated cementation. In principle, more diffuse flow within weathered granites could contribute to groundwater flow in the near subsurface, but the heterogeneous nature of weathering and the outflow of geothermal fluids indicate that up-fault flow connectivity, either within the V-P Fault rocks or damage zone, is effectively a pre-requisite of the La Garriga geothermal system. The best examples of these are from the S1 borehole (IGME, 1982), which extends to depths of nearly 1 km, and given the vertical orientation of the borehole and the steep dip of the V-P Fault (ca 70º), must be within ca 200 m of the main fault surface and well within the intensely deformed damage zone of the fault. The presence of vuggy vein infills attests to the flow connectivity of the associated fracture system, but in the absence of flow data (e.g., flow rate, hydraulic conductivity), there is no means of directly defining the flow properties of the system.

Therefore, we use a method in which groundwater parameters are defined analytically from empirically derived measures of fracture aperture (perpendicular opening) and spacing (perpendicular distance). This approach assumes that the concepts of equivalent permeability and representative elementary volume (REV) are tenable at the scale of the flow and transport volume of interest (Zimmerman and Bodvarrson 1996; Odling et al. 1999; Müller et al. 2010). Porosity (p), permeability (k), and hydraulic conductivity (K) are estimated using the cubic flow law (e.g., NRC 1996; Zimmerman and Bodvarsson 1996; Schwartz and Zhang 2003), assuming horizontal flow through regular spaced fractures with constant aperture (Reiss 1980; Motyka 1998; Müller et al. 2010 and refs therein; Fig. 12). This method utilises the cubic flow law, in which flow velocities relate to the cube of the aperture and are only linearly dependent on spacing. Whilst this approach is a gross simplification of the structural complexity of the fracture networks concerned, it provides a very general approximation of the potential flow parameters of different components of the fracture system, not including the weathering-related poro-perm contributions discussed earlier.

The available data used in this study derive from estimates of fracture spacing and aperture, with the latter derived from vein aperture and/or vein thickness measurements, a potential shortcoming we will consider later. Taken together, these data indicate very significant combinations of apertures or thicknesses and densities of fractures adjacent to the fault. The cumulative fracture porosity (including filled and infilled fractures) is, however, very modest with values of between 1%-0.1% porosity. The highest values of fracture porosity are recorded within the lenticular fault zone in the centre of the study area, which is interpreted to have previously been a relay. Progressively lower fracture porosities are recorded within the damage zones and the fault core, in particular, with some dykes marked by high fracture porosities, but with very low apertures.

Translating these geometric measures of aperture/thickness and fracture spacing into flow properties such as bulk permeability (m^2) and hydraulic conductivity (m/d), suggests that flow is likely to be localized within the V-P relay zone and adjacent to the Paleogene thrust, an outcome which highlights the importance of both structures in controlling up-fault and along-fault flow. The granodioritic outcrops provide a very broad spread in derived permeability, whereas the relay area is the most permeable and conductive zone overall. Despite the relationship between fracture density and proximity to the V fault, the importance of relay zone and thrust surface reflects the pre-eminence of dilatancy and aperture in estimating flow properties. Whilst these estimates provide some indication of the localization of flow within different components of the fracture system, the flow properties estimated have utilized the combined aperture and infill rather than the prevailing aperture at any given moment in time. Insofar as the thickness of fractures could conceivably derive from many hundreds or more increments of opening or valving of fractures, perhaps related to individual earthquakes, the flow properties should not be taken as representative of the prevailing flow properties. Estimates of 2-3 orders of magnitude lower are perhaps much more likely, but would, nevertheless, still indicate fracture permeabilities in excess of 1 Darcy (equivalent to bulk permeabilities of 10^{-12} m^2). Another factor that is not indexed in these simple calculations of permeability is that whilst carbonate infills demonstrate the circulation of geothermal fluid, they also reflect the ability of fractures to self-seal. This self-sealing could inhibit flow, but valving of fluids during multiple slip events or earthquakes often operates on the same fractures, which have, in any case, vuggy, and therefore weaker infills (Cantarero et al., 2010; Facca and Tonani, 1967). Given the prolonged and ongoing activity of self-sealing fractures, there is every reason to expect self-sealing to be a transient phenomenon.

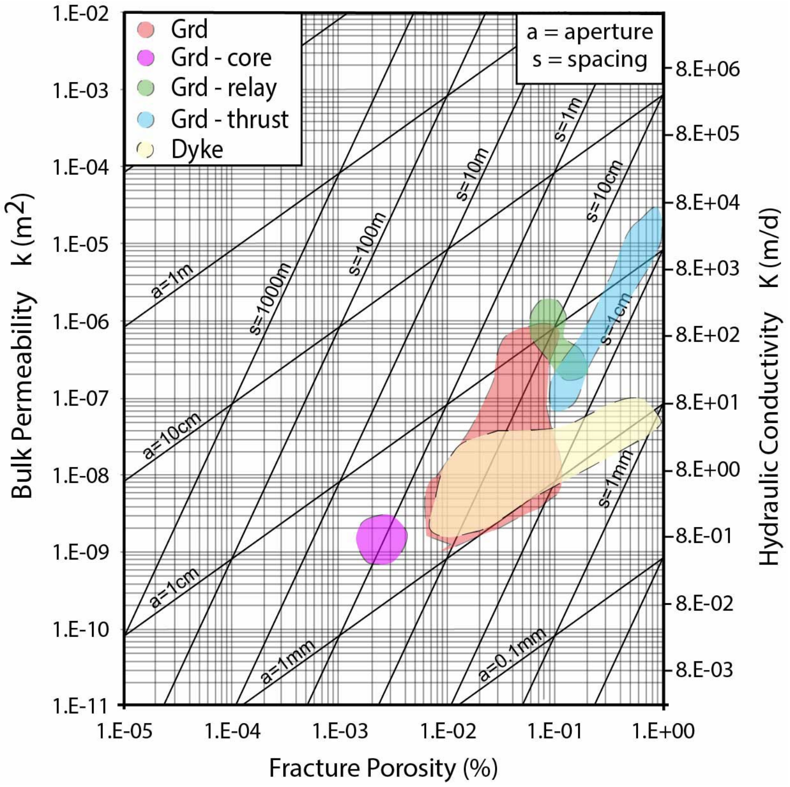

Figure 12. Fracture spacing (s) vs fracture aperture (a) data for the study area, in which aperture is taken to be the cumulative fracture porosity (including filled and infilled fractures). The colors of the granodioritic unit measurements locate the samples in the fault core, in the relay zone, and close to the Alpine Thrust. These data are also plotted within estimated bulk permeability, fracture porosity and hydraulic conductivity, using the method of Reiss (1980) assuming horizontal flow through regular spaced fractures with constant aperture. This approach provides very general estimates of fracture-controlled flow properties, which are, however, subject to very significant uncertainties (see text for details).

7. Discussion

7.1. Alpine structure of the eastern margin of the Vallès-Penedès Basin.

The present-day structure of the Catalan Coastal Ranges predominantly reflects normal faulting arising from Neogene extensional tectonics, which post-dates and cuts Paleogene structures developed during compressional Alpine deformation (Marcén et al., 2018). Previous authors investigating the structural evolution of the Catalan Coastal Ranges have suggested that the V-P Fault is the result of the negative inversion of thrusts during Neogene extension (Anadón et al., 1979; Fontboté, 1954; Roca et al., 1999), but there is no consensus regarding the geometric relationship between the Prelitoral Thrust and the V-P Fault.

Our analysis of the available data confirms that the V-P Fault is a steeply dipping structure, with dips generally between 60^0 and 70^0 apart from more inclined surfaces associated with a relay at La Garriga town. This geometry is compatible with that of a bifurcating upwards normal fault marked by a breached relay at the surface (Giba et al. 2012; Roche et al. 2021).

Seismic evidence indicates approximately planar faults, albeit with some limited shallowing in the upper 10 km of the crust (Roca et al. 1999). The presence of hangingwall rollover has been interpreted to suggest a detachment at depths of 13-15 km (Roca and Guimera, 1992), but direct evidence from depth-converted seismic sections is lacking and similar deformations are also typical of established flexural-isostatic models of planar faults (e.g. Roberts & Yielding 1994). In this background context, we favour a planar fault model down to depths exceeding 10 km, a scenario that is commonplace in most low-strain intra-cratonic rift systems, such as the North Sea and the Basin and Range (e.g. King et al. 1988; Kusznir and Ziegler 1992), and is capable of generating the tilted fault blocks of the Catalan Coastal Ranges (Roca et al. 1999), together with the hangingwall subsidence and footwall uplift associated with individual faults.

In these circumstances, we propose two alternatives for explaining the current spatial relationship between the Paleogene thrust and the V-P Fault. First, the geometrical current configuration could simply arise from a normal fault offsetting a previous shallow dipping thrust which is therefore only exposed within the footwall of the normal fault but would have a deeper expression within the hangingwall fault block. An alternative model is that the Paleogene thrust is a footwall short-cut structure arising from the inversion of any pre-Tertiary expression of the V-P normal fault. Distinguishing between these models is not easy given the available constraints but insofar as the thrust does not appear to steepen and root into the V-P Fault, a cross-cutting relationship is favored. Whichever of these models is correct, both involve a deeply rooted normal fault extending into basement, circumstances which promote the emergence of a high enthalpy geothermal systems developed along the V-P Fault.

Although the Paleogene and Neogene tectonic evolution of the Catalan Coastal Ranges has been well studied, there are much fewer constraints on the Pliocene and Quaternary tectonic evolution of the region (Masana, 1996). The general consensus is that the main phase of normal faulting in the V-P Basin began in Late Oligocene times, at the latest, and continued into the Late Miocene

(Tortonian), particularly along the V-P Fault (e.g. Bartrina et al. 1992; Roca et al. 1999). Thereafter, decreases in across-fault sequence growth have been attributed to the predominance of late rift-related thermal subsidence and sedimentation, and the accommodation of lower rates of crustal extension, principally by the cessation of movement on most faults and a decreased level of fault activity along the larger faults, such as the V-P Fault and the Barcelona Fault (Masana, 1995, 1994; Roca et al. 1999). Small faults within the Pliocene and Lower Quaternary are sparse, attesting to the decreased intensity and activity of normal faulting in that period. Associated seismicity within the Catalan Coastal Range is considered to be low (Massana, 1994), with several earthquakes of M < 4 every year, and whilst there have been no recorded earthquakes greater than M5, two historical earthquakes with intensities of VII and VII-VIII (corresponding to M6.0-6.8) have occurred on or adjacent to the V-P Fault (de Galdeano et al. 2020). Despite this relatively low level of activity, these earthquakes and the protracted history of the V-P Fault provide support for fault reactivation and associated fluid circulation, a scenario we consider later in the context of the geothermal systems of La Garriga and Caldes de Montbui.

7.1.1. Fault trace and displacement geometry of the V-P Fault.

Constraints from mapping and geophysical data indicate that the V-P Fault has a maximum displacement of ca 5 km and a trace length of 100 km (Bartrina et al., 1992; Gallart et al., 1997; Gaspar-Escribano et al., 2004; Gómez and Guimerà, 1999; Juez-Larré and Andriessen, 2006; Roca and Guimerà, 1992; Sàbat et al., 1995; Vidal et al., 1995), scaling properties that are consistent with existing empirical constraints for normal faults (Nicol et al. 2020).

Lateral changes in displacement along the V-P Fault are supported by lower displacements (<3 km) in the study area, the presence of exposed fault tips at either end of the fault, the narrowing of the V-P Basin towards the NE and SW, and evidence on seismic profiles for a decrease in the basement depth of the V-P Basin towards the NE (Roca, 1992). Towards the eastern tip of the fault, the prevailing hangingwall topography also dips towards the SW, with associated river systems sourced directly from the footwall mountains in the north and curving towards the SW in the south.

Although the mapped trace of the V-P Fault is relatively simple on regional scale maps (Fig. 1), closer examination indicates that it is marked by fault bends and steps that are developed at and below km-scales. At Caldes de Montbui, towards the eastern limit of the V-P Fault, the trace is marked by non-aligned linear segments connected by fault bends. A very similar structure has been defined in the study area as the La Garriga relay zone, which has a width of 650 m and an overlap length of 2000 m, consistent with the scaling relationship of relays along large faults (Fossen and Rotevatn, 2016).

Combining the displacement and relay dimensions, and comparing them with empirical quantitative constraints of large published relay databases, strongly suggests that the relay is breached and, most likely, doubly breached to form a lenticular zone of fault-related deformation because the rapid transfer of 1.5 km scale displacements is not compatible with an intact relay at that 1-2 km scale (Fig. 13).

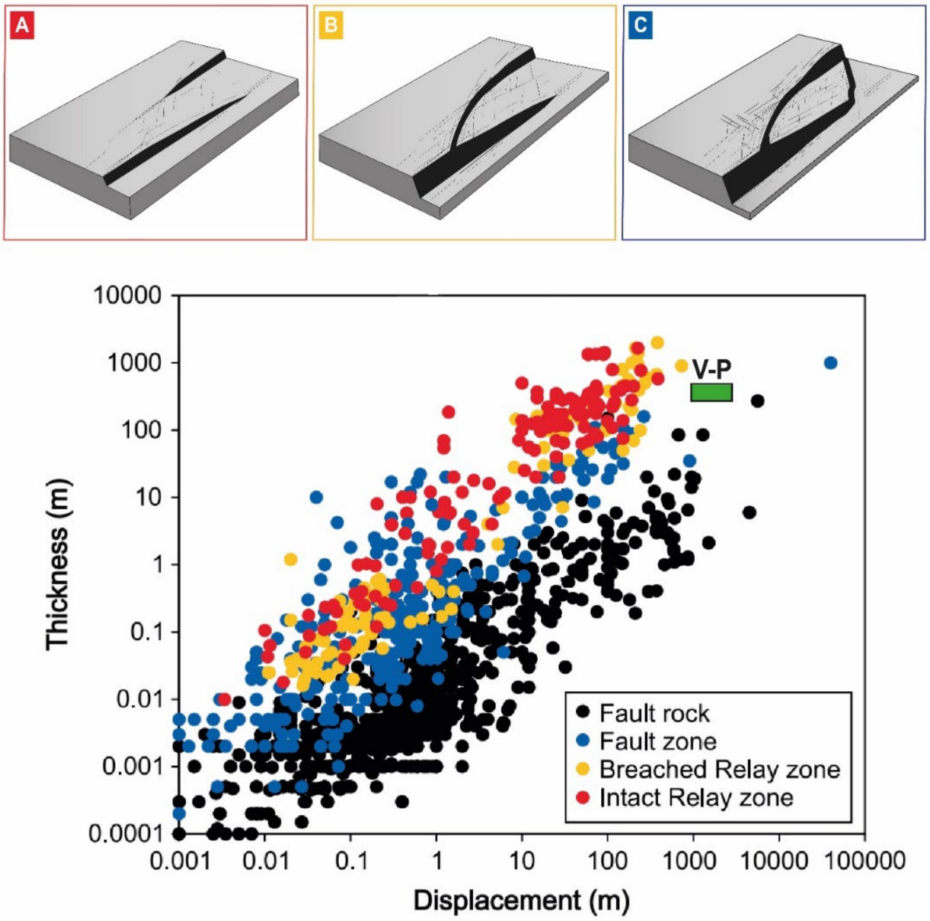

Figure 13. *A) Unbreached relay ramp displaying ramp-related fracturing and deformation. The thickness (T), or segment perpendicular separation, is shown. (B) Breached relay ramp in which continuous (i.e. ramp-related) deformations still accommodate much of the displacement transfer between segments. (C) Doubly-breached relay ramp, with strongly deformed fault lens. (D) Displacement vs thickness plot for different components of fault zones, including intact relay zones (red), breached relay zones (orange), fault zones (blue; including intact relays through to fault lenses) and fault rock (black). The scaling of the V-P fault zone at La Garriga is consistent with the presence of strongly fractured host rock and fault rock.*

Our work also indicates that relay breaching promotes the fracturing of adjacent granite host rocks, in particular, circumstances that provide a means of generating steeply inclined potential pathways along the mapped relay axis (Fossen and Rotevatn, 2016)Walsh et al. 2018). Analysis of the relay within La Garriga highlights the intense fracturing associated with the fault zone, in which faults that are parallel and perpendicular to the main V-F Fault provide a basis for generating a fracture network which is the locus for fluid flow, an issue we consider below.

Very indirect support for the presence of a relay adjacent to both the La Garriga and Caldes de Montbui geothermal systems is provided by the transecting rivers at those locations, an association that has been advocated in other active continental rifts, such as the Sperchios Basin, Central Greece (Eliet and Gawthorpe 1995), and the Gedz Graben, Western Turkey (Dart et al. 1995). The presence of river systems associated with relays, therefore, comes with the potential of dispersing geothermal fluids within Quaternary river sediments, a scenario which is known to have occurred at La Garriga.

7.1.2. *Basinal context for geothermal systems within Vallès-Penedès Basin*

Located within the Oligocene-early Miocene to recent Vallès-Penedès Basin, the Vallès site benefits from the presence of a relatively thick basin fill (up to 3 km) deposited upon mainly Hercynian metasediments and granites. Development of this 50 km wide half-graben is in the context of a much wider fault system extending across the Catalan Coastal Ranges (CCR) into the Valencia Trough (Fig. 7). The NE-trending graben is marked by emergent and faulted basin margins bounding domino-style faulting, with internal deformation of individual dominoes generating hangingwall rollover, footwall uplift, and the rotation of fault blocks.

The generation of the basin- and range--type terrains, and the deposition of siliciclastic sediments containing substantial thicknesses of sometimes relatively high poro-perm alluvial/fluvial sandstones (up to ca 2.5 km thick), provides a basis for the ingress of groundwater and its retention within basinal sequences. On the other hand, basement rocks underlying the V-P Basin Miocene infill are, however, volumetrically more significant than the basin fill sequence and could, therefore, represent the best means of both recharging the basinal fluid system and sourcing hotter fluids. For example, Mesozoic carbonate-dominated sequences are up to 2 km thick and comprise fractured and karstified limestone sequences in the southern and southwestern part of the V-P basins (ca 30 km from the study area) and within the Garraf-Montenegre, which separates the V-P and the Barcelona Basins (Baqués et al. 2012; Marin et al. 2021). Previous work has indicated multiple phases of meteoric percolation and fracturing processes within these limestones, with karst development extending from the pre-rift to late-rift phases of Neogene rifting (Baques et al. 2012; Marin et al. 2021). Underlying Variscan basement comprises Cambrian to Carboniferous slates together with Carboniferous to Permian granitoids (Marin et al. 2021), broadly corresponding to the metamorphic and granitoid basement rocks of the study area. Ongoing deformation arising from continued extension and associated earthquake activity also provides a means of driving fluids during seismic cycles through a variety of mechanisms including seismic valving or pumping. The accommodation of groundwater flow to significant depths is facilitated by the extensional nature of the basin, the porous nature of much of the basin fill and the fractured and karstified nature of underlying Mesozoic and Variscan basement rocks. These circumstances together with the tectonically and volcanically active (the volcanic region of La Garrotxa is located 60 km northeast of La Garriga) setting of the area provides an excellent basis for a system characterized by high geothermal gradients and hydrodynamic drives with hot springs providing groundwater temperatures of up to ca 60^0C and recorded downhole temperatures of up to 90^0C at depths of 1 km.

Localization of hot springs with elevated temperatures within the CCR is always associated with faulting (Canals et al., 1989; Cardellach et al., 2002; Fernàndez and Banda, 1988; Mitjanas et al., 2021). Faults evidently provide the optimal means of transporting hot aqueous fluids from depth up to the surface. The along-fault migration of fluids is sufficiently rapid to preserve high temperatures, circumstances which are not satisfied by slower fluid migration through syn-rift sediments or basement rocks (Fig. 14). Therefore, fluid flow is promoted by the tectonically active nature of the system and by the associated deformation processes.

The response of different host rocks to the accommodation of displacement is very distinct, with adjacent granites marked by cataclastic fault rocks and damage zones that are dilational in nature but with more porous syn-rift sediments expected to be marked by deformation bands and compactive fault rocks that are usually detrimental to across-fault flow but can nevertheless be pathways for up-fault flow. Support for these prevailing fault rock distributions is provided by the presence of cataclastic gouge adjacent to syn-rift host rocks within boreholes and the prevalence of fracture-controlled flow within the granitic footwall.

The longevity of the flow system is very difficult to define, but the pervasive nature of the alteration of the granite host rocks is marked by the sericitization of feldspar, the retrogression of biotite to chlorite and by the precipitation of a variety of other alteration minerals. Another feature supporting the prolonged activity of the hydrothermal system is the intensity of vein filled fractures that have multiple orientations and are often vuggy. These types of fracture system attest to the overpressured nature of the associated thermal waters and strongly elevated downhole temperatures suggesting along fault geothermal gradients of nearly 100^{0}C/km.

7.1.3. 3D conceptual model of the Vallès geothermal system

The development of geothermal systems adjacent to faults within extensional basins is a well-established phenomenon (Curewitz and Karson, 1997; Sibson, 2001; Fairley and Hinds, 2004a, b; Walsh et al. 2018 and references therein). Crustal thinning is accompanied by increases in geothermal gradient and the potential for the deeply penetrating convective flow systems with a hydrodynamic system supplied by the downward ingress of groundwater through faults, syn-rift, or hydrostatically pressured basement. Whilst the sinking of fluids will be facilitated by increases in salinity, analysis of the thermal waters at La Garriga spa does not suggest the presence of heavy brines (López-Geta et al., 2002). Within the Vallès-Penedès basin, the migration pathways are unclear, with the potential for north- and northwestward migration into the basin via hangingwall syn-rift sequences and karstified Mesozoic limestones or via uplifted footwall, mainly granitic, blocks in the southeast, or with south- to southwestward migration pathways from footwall Paleozoic metamorphic/granites, Triassic sediments or perhaps even volcanics much further to the NE. Given the prevalence of clastic syn-rift sequences and underlying fractured/karstified pre-rift rocks in the V-P basin, there are strong grounds for the sourcing of groundwater for the very localized geothermal systems along the V-P Fault. The main concerns thereafter are the hydrodynamic drive and localization of fluids within the system.

The available evidence suggests that whilst the V-P fault system basin was not as tectonically active in Pliocene-recent times, compared to its main period of activity in late Oligocene to late Miocene times, historical earthquakes with magnitudes of up to 6.8 have occurred, and the fault is considered active. Recent estimates of the seismic parameters of the so-called Montseny Fault (de Galdeano et al. 2020), which is the northern end of the V-P Fault, suggest slip rates of 0.05-0.13 mm/year arising from earthquakes with maximum magnitudes of 6.7-6.8 and mean recurrence intervals of ca 26,000 years. These characteristics are very similar to faults within the Basin and Range, from which seismic pumping models of fault-related fluid flow have been advanced (Muir-Wood & King 1993).

Seismic pumping involves the interseismic accumulation of dilations due to fracturing and poro-elastic effects within host-rock volumes surrounding normal faults (Walsh et al., 2018). Co-seismic deformation is then marked by the imposition of compressional strains subscribing to elastic dislocation theory which involve the expulsion of considerable volumes of fluid during individual earthquake events (Sibson et al. 1975; Blundell 2002). Muir-Wood and King (1993) showed that predicted co-seismic porosity losses are consistent with accentuated surface flow during major earthquakes in the Basin and Range province, with, for example, volumetric changes of 0.3 km^3 of water expelled during the Borah Peak 1983 earthquake (M~6.9). This earthquake occurred on the Lost River Fault which has a maximum displacement of >4km requiring ca 1000 similar-sized events for regional recurrence intervals of 20,000 years over the lifetime of the Basin and Range. This scenario provides a basis for the draw-down and driving of fluid volumes of ca 3 x $10^2 km^3$ within the host rocks surrounding a normal fault which is very similar to that of the V-P Fault. Whilst this model could make an important potential contribution to the hydrodynamics of the V-P Basin it does not, on its own, provide a rationale for the localization of flow along the V-P fault itself. For this we advocate a model for fault-driven fluid flow referred to as seismic pulsing, in which earthquake slip and frictional sliding causes transient dilation (i.e., opening) and the pulsing of fluids up the fault surface (Wilkins and Naruk, 2007), a process that is similar to the seismic suction pump model described by others (Rudnicki and Chen, 1988; Grueschow et al., 2003). Estimates of transient dilation for the V-P Fault, a 100 km long structure with a time-averaged slip rate of 0.1 to 1mm/year, range between 10 km^3 to 100 km^3, corresponding to large flow volumes which could be even more strongly localized because of along-fault relays and lenses.

Even assuming the cessation of fault slip along the V-P Fault in Pliocene to recent times, the basin will retain much of the syn-rift hydrodynamic regime, including structural, thermal and pore-fluid pressure drives. One of the principal mechanisms for up-fault flow is fault valving which is exclusively driven by the migration of higher pressure (i.e. deep and warmer) fluids when fluid pressures lead to mechanical failure of fault seals, a scenario which can occur within basins that are not tectonically active (Phillips 1972, Sibson 1990, 1992; Walsh et al. 2018). Another potential mechanism is even simpler, insofar as it requires passive up-fault flow along preferred flow conduits at rates which match the build up of fluids at depth. Whichever combination of models applies, the basic requirement for structurally controlled flow localization at particular sites is complexity and heterogeneity of structure. What this study has shown is that hydrothermal fluid flow is developed preferentially towards the intersection of a Paleogene thrust and the V-P Fault. The basic configuration and trace of this thrust suggests that its intersection line with the normal fault will plunge towards the centre of the fault away from the mapped branch points, a scenario which will lead to preferential flow towards the ends of the thrust. Perhaps more importantly for the La Garriga geothermal system, a major step in the Vallès Fault is characterized by accentuated fault damage, veining, and fluid flow. This scenario is consistent with evolutionary models for the growth and breaching of relays, which are often considered to be the locus for up-fault fluid flow (e.g. Rotevatn & Bastesen 2012; Fossen & Rotevatn, 2016; Kyne et al. 2019). The importance of this structure is clearly reflected in the thermal structure of the area and accentuated porosity and permeability arising from higher density fracture systems and meshes, providing conduits for the upward flow of hydrothermal fluid (Fig. 14), which in the study area provides groundwater of ca 60^{0}C, with recorded downhole temperatures of up to 90^{0}C at depths of 1 km.

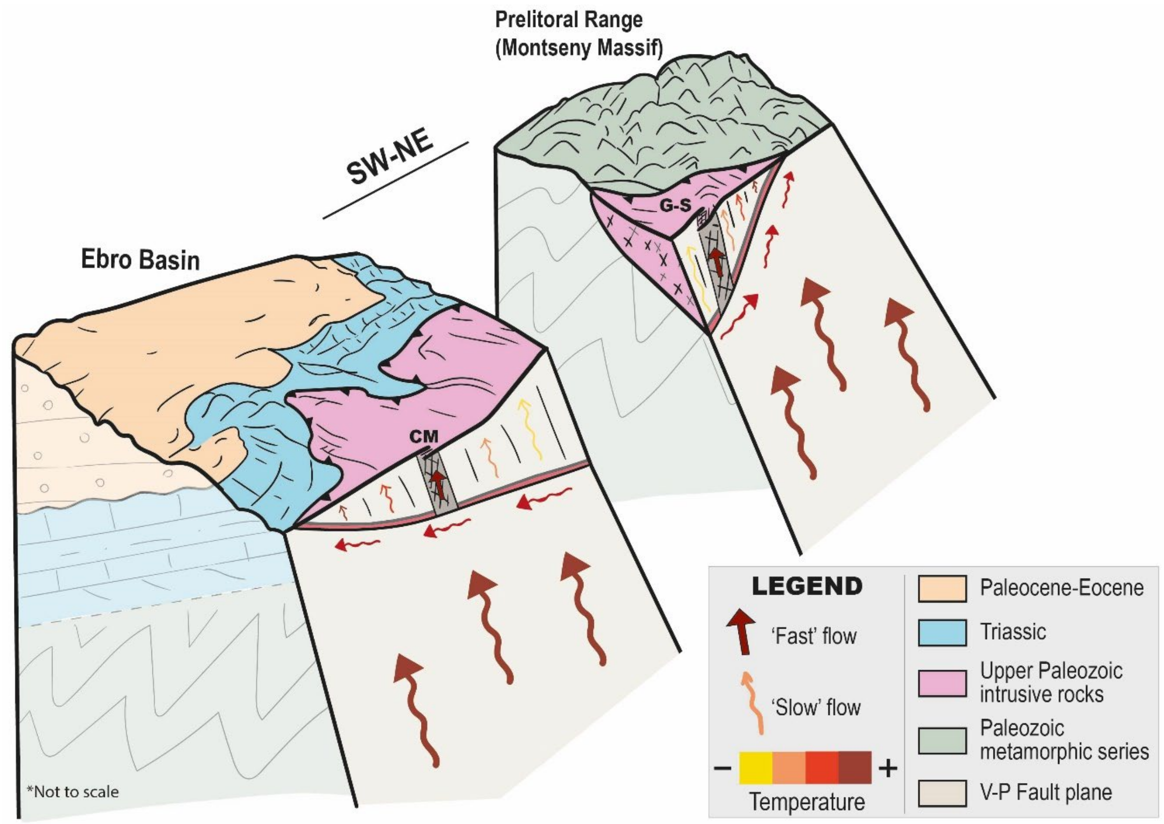

Figure 14. *Geothermal conceptual model of the Caldes de Montbui (CM) – La Garriga and Samalús (G-S) system. Curvilinear arrows indicate the slower ascend of fluids, and their color, their relative temperature. The red straight arrows indicate the preferential channels for hydrothermal fluid upwelling. See text for details.*

8. Conclusions

The integration of earlier and newly acquired geological and geophysical data provides the basis for an improved conceptual model of the Vallès Basin geothermal system. The model incorporates better characterization of the structural controls on fluid flow, with the following principal conclusions:

- There is a direct relationship between the localization of geothermal flow (e.g. 60^{0}C at surface and 90^{0}C at 1 km depths), associated weathering and cementation, and the locations of increased structural complexity along major normal faults, such as the V-P Fault.
- Complexity of fault zone structure of normal faults is attributed to fault segmentation and the breaching of relay ramps, to provide enhanced intensities of dilational and hybrid fractures, surpassing those of conventional along-fault damage zones.
- The nature and degree of fracturing is conditioned by proximity to the main fault and associated structural complexities, and is accentuated within otherwise low porosity/permeability basement host rocks, and granites in particular.

- The local plumbing of fluid flow along the Vallès-Penedès Fault is also interpreted to be affected by lateral flow along the intersection of later normal faults and an earlier Paleogene thrust, a configuration which helps to further localized flow.
- Networks of dilational and hybrid fractures are the locus for fluid flow, with the self-sealing of individual fractures a transient feature of a system characterized by the valving of overpressured fluids and the seismic pumping associated with earthquake events.
- By analogy with other active normal fault systems, the Vallès Basin is capable of providing sustainable geothermal flow systems, with recharge zones provided by faults and the emergent footwalls of fractured basement rocks, and structurally complex discharge zones along normal faults enabling the rapid upward flow of hot geothermal fluids.

9. Acknowledgements

Pep Albert for providing the borehole samples; ICGC for providing the data of H/V method; Technical University of Freiberg and Dra. Janna Börner for the petrophysical analysis support.

10. Funding

Research at University of Barcelona was funded by the GEO-URBAN project (ERANET-GEOTHERMICA project no. 73117 and PCI2018-092943 Spanish Government - Ministerio de Ciencia, Innovación y Universidades); and the PIXIL project (project no. EFA362/19, co-financed by the INTERREG POCTEFA program of the European Regional Development Fund, and the University of Barcelona).

Research at University College Dublin was supported by the GEO-URBAN Project through the Geothermica Programme, with funding from the Geological Survey Ireland, and was also part-funded by a research grant from Science Foundation Ireland (SFI) under grant number 13/RC/2092 and co-funded under the European Regional Development Fund.

11. Data availability

Datasets related to this article can be obtained asking to the corresponding author (gmitjanas@ub.edu).

12. References

Achtziger-Zupančič, P., Loew, S., Hiller, A., 2017. Factors controlling the permeability distribution in fault vein zones surrounding granitic intrusions (Ore Mountains/Germany). J Geophys Res Solid Earth 122, 1876–1899. https://doi.org/10.1002/2016JB013619

Anadon, P., Cabrera, L., Guimera, J., Santanach, P., 1985. Paleogene strike-slip deformation and sedimentation along the southeastern margin of the Ebro Basin. Strike-slip deformation, basin formation, and sedimentation 303–317. https://doi.org/10.2110/pec.85.37.0303

Anadón, P., Colombo, F., Esteban, M., Marzo, M., Robles, S., 1979. Evolución tectonoestratigráfica de los Catalánides. Acta geológica hispánica 14, 242–270.

Anderson, J.L., Osborne, R.H., Palmer, D.F., 1983. Cataclastic rocks of the San Gabriel fault - An expression of deformation at deepr crustal levels in the San Andreas fault zone. Tectonophysics 98, 209–251.

Bard, P.-Y., 1998. Microtremor measurement: a tool for site effect estimation? In: Second International Symposium on the Effects of Surface Geology on Seismic Motion. Yokohama, Japan, pp. 1251–1279.

Bard, P.-Y., 1985. Les effets de site d'origine structurale: Principaux résultats experimentaux et théoriques., in: Davidovici, V. (Ed.), Genie Parasismique. Presses de l'école nationale des ponts et chaussées., pp. 223–238.

Bartrina, M.T., Cabrera, L., Guimerà, J., Roca, E., Jurado, M.J., 1992. Evolution of the central Catalan margin of the Valencia trough (western Mediterranean). Tectonophysics 203, 219–247.

Bellanger, M., Hermant, B., Galibert, S., Auxiètre, J., 2019. Fault-controlled hydrothermal system associated with major Crustal Fault Zone: future drilling target to assess the deep geothermal potential – The Sioule license project. European Geothermal Congress 2019, Den Haag, The Netherlands, 11-14 June 2019 1–10.

Benjumea, B., Macau, A., Gabas, A., Bellmunt, F., Figueras, S., Cirés, J., 2011. Integrated geophysical profiles and H/V microtremor measurements for subsoil characterization. Near Surface Geophysics 9, 413–425.

Benjumea, B., Macau, A., Gabàs, A., Esquerda, M., Figueras, S., 2014. Improving near surface characterization by combining reprocessed vintage seismic and geophysical passive datasets. Near Surface Geoscience 2014 - 20th European Meeting of Environmental and Engineering Geophysics 14–18.

Bertrand, L., 2017. Etude des réservoirs géothermiques développés dans le socle et à l'interface avec les formations sédimentaires. Université de Lorraine.

Bertrand, L., le Garzic, E., Géraud, Y., Diraison, M., 2013. Fractured crystalline reservoir: A field analog analysis on Tamariu's granite (Catalonian Coastal Ranges). 2nd EAGE Workshop Naturally Fractured Reservoirs: Naturally Fractured Reservoirs in Real Life. https://doi.org/10.3997/2214-4609.20132004

Betlem, P., Birchall, T., Ogata, K., Park, J., Skurtveit, E., Senger, K., 2020. Digital drill core models: Structure-from-motion as a tool for the characterisation, orientation, and digital archiving of drill core samples. Remote Sens (Basel) 12. https://doi.org/10.3390/rs12020330

Cabrera, L., Calvet, F., 1996. Onshore Neogene record in NE Spain: Vallès–Penedès and El Camp half-grabens (NW Mediterranean), in: In P. Friend & C. Dabrio (Ed.), Tertiary Basins of Spain: The Stratigraphic Record of Crustal Kinematics. Cambridge University Press, pp. 97–105.

Caine, J.S., Evans, J.P., Forster, C.B., 1996. Fault zone architecture and permeability structure. Geology 24, 1025–1028.

Camanni, G., Roche, V., Childs, C., Manzocchi, T., Walsh, J., Conneally, J., Saqab, M.M., Delogkos, E., 2019. The three-dimensional geometry of relay zones within segmented normal faults. J Struct Geol 129, 103895. https://doi.org/10.1016/j.jsg.2019.103895

Canals, A., Albert, J., Ayora, C., 1989. El sistema geotérmico de la Garriga-Samalús: : comparaciones con sistemas hidrotermales fósiles. Geogaceta.

Cantarero, I., Lanari, P., Vidal, O., Alías, G., Travé, A., Baqués, V., 2014. Long-term fluid circulation in extensional faults in the central Catalan Coastal Ranges: P-T constraints from neoformed chlorite and

K-white mica. International Journal of Earth Sciences 103, 165–188. https://doi.org/10.1007/s00531-013-0963-8

Cantarero, I., Travé, A., Alías, G., Baqués, V., 2010. Pedogenic products sealing normal faults (Barcelona Plain, NE Spain). J Geochem Explor 106, 44–52. https://doi.org/10.1016/j.gexplo.2010.02.004

Cardellach, E., Canals, A., Grandia, F., 2002. Recurrent hydrothermal activity induced by successive extensional episodes: The case of the Berta F-(Pb-Zn) vein system (NE Spain). Ore Geol Rev 22, 133–141.

Cartwright, J.A., Mansfield, C., Trudgill, B., 1996. The growth of normal faults by segment linkage. Geol Soc Spec Publ 99, 163–177. https://doi.org/10.1144/GSL.SP.1996.099.01.13

Childs, C., Watterson, J., Walsh, J.J., 1995. Fault overlap zones within developing normal fault systems. Journal - Geological Society (London) 152, 535–549. https://doi.org/10.1144/gsjgs.152.3.0535

Cloos, H., 1922. Tektonik und Magma: Untersuchungen zur Geologie der Tiefen.

CloudCompare [GPL software], 2021.

Duan, Q., Yang, X., Chen, J., 2017. Hydraulic properties of a low permeable rupture zone on the Yingxiu-Beichuan Fault activated during the Wenchuan earthquake, China: Implications for fluid conduction, fault sealing, and dynamic weakening mechanisms. Tectonophysics 721, 123–142. https://doi.org/10.1016/j.tecto.2017.10.002

Duwiquet, H., Arbaret, L., Guillou-Frottier, L., Heap, M.J., Bellanger, M., 2019. On the geothermal potential of crustal fault zones: a case study from the Pontgibaud area (French Massif Central, France). Geothermal Energy 7. https://doi.org/10.1186/s40517-019-0150-7

Duwiquet, H., Guillou-Frottier, L., Arbaret, L., Bellanger, M., Guillon, T., Heap, M.J., 2021. Crustal Fault Zones (CFZ) as Geothermal Power Systems: A Preliminary 3D THM Model Constrained by a Multidisciplinary Approach. Geofluids 2021. https://doi.org/10.1155/2021/8855632

Facca, G., Tonani, F., 1967. The self-sealing geothermal field. Bulletin Volcanologique 30, 271–273. https://doi.org/10.1007/BF02597674

Faulds, J.E., Hinz, N.H., 2015. Favorable Tectonic and Structural Settings of Geothermal Systems in the Great Basin Region , Western USA: Proxies for Discovering Blind Geothermal Systems. World Geothermal Congress 2015 1–6.

Faulkner, D.R., Jackson, C.A.L., Lunn, R.J., Schlische, R.W., Shipton, Z.K., Wibberley, C.A.J., Withjack, M.O., 2010. A review of recent developments concerning the structure, mechanics and fluid flow properties of fault zones. J Struct Geol 32, 1557–1575. https://doi.org/10.1016/j.jsg.2010.06.009

Fernàndez, M., Banda, E., 1990. Geothermal Anomalies in the Vallès-Penedès graben master fault: convection through the horst as a possible mechanism. J Geophys Res 95, 4887–4894.

Fernàndez, M., Banda, E., 1988. Aproximacion a la anomalia geotérmica de La Garriga - Samalus (Vallès - Penedès). Acta Geológica Hispánica 23, 1–20.

Fontboté, J.M., 1954. Sobre la evolución tectónica de la depresión del Vallés-Pened-es. Publ. Museu Sabadell, Sabadell.

Fontboté, J.M., Guimerà, J., Roca, E., Sàbat, F., Santanach, P., Fernández-Ortigosa, F., 1990. The Cenozoic geodynamic evolution of the Valencia trough (Western mediterranean). Rev. Soc. Geol. Esp 3, 249–259.

Fossen, H., Rotevatn, A., 2016. Fault linkage and relay structures in extensional settings-A review. Earth Sci Rev 154, 14–28. https://doi.org/10.1016/j.earscirev.2015.11.014

Gabàs, A., Macau, A., Benjumea, B., Queralt, P., Ledo, J., Figueras, S., Marcuello, A., 2016. Joint Audio-Magnetotelluric and Passive Seismic Imaging of the Cerdanya Basin. Surv Geophys 37, 897–921.

Gallart, J., Vidal, N., Daiiobeitia, J.J., 1997. The ESCI Valencia Trough vertical reflection experiment : a seismic image of the crust from the NE Iberian Peninsula to the Western Lateral variations in the deep crustal structure at the Iberian margin of the Valencia trough imaged from seismic reflectio.

Gaspar-Escribano, J.M., 2003. Tectonic modeling of the Catalan Coastal Ranges (NE Spain) and adjacent areas. Vrije Univ. Amsterdam.

Gaspar-Escribano, J.M., Garcia-Castellanos, D., Roca, E., Cloetingh, E., 2004. Cenozoic vertical motions of the Catalan Coastal Ranges (NE Spain): The role of tectonics, isostasy, and surface transport. Tectonics 23, 1–18.

Géraud, Y., Rosener, M., Surma, F., Place, J., Le Garzic, É., Diraison, M., 2010. Physical properties of fault zones within a granite body: Example of the Soultz-sous-Forêts geothermal site. Comptes Rendus - Geoscience 342, 566–574. https://doi.org/10.1016/j.crte.2010.02.002

Gómez, M., Guimerà, J., 1999. Estructura Alpina de la Serra de Miramar y del NE de Las Muntanyes de Prades (Cadena Costera Catalana). Rev. Soc. Geol. Esp 12, 405–418.

Guimerá, J., 1984. Palaeogene evolution of deformation in the northeastern Iberian Peninsula. Geol Mag 121, 413–420. https://doi.org/10.1017/S0016756800029940

Guimerá, J., Santanach, P., 1978. Sobre la compresión alpina en el sector central de las Cadenas Costeras Catalanas. Acta geológica hispánica 13, 33–42.

Haines, S., Lynch, E., Mulch, A., Valley, J.W., van der Pluijm, B., 2016. Meteoric fluid infiltration in crustal-scale normal fault systems as indicated by δ18O and δ2H geochemistry and 40Ar/39Ar dating of neoformed clays in brittle fault rocks. Lithosphere 8, 587–600. https://doi.org/10.1130/L483.1

ICGC, 2006. Vallès Oriental. Mapa geològic comarcal de Catalunya 1:50.000.

ICGC, 2002. Mapa Geològic de Catalunya 1:250.000.

IGME, 1986. Proyecto de seguimiento geológico del sonde de reconocimiento geotérmico SAMALUS-6 (1000 m) (Vallès-Barcelona).

IGME, 1984. Proyecto de investigación geotérmica en el Vallés mediante sondeos de reconocimiento y síntesis hidrogeotérmica. Control geotermico de los sondeos SAMALUS 2, 3, 4 y 5.

IGME, 1982. Informe sobre el seguimiento técnico del sondeo SAMALUS-1.

IGME, 1977. Fase preliminar de prospección de recursos geotérmicos de baja entalpía en el Vallés (Barcelona).

IGME, 1974. La Garriga (364). Mapa geológico de España 1:50 000:

Juez-Larré, J., Andriessen, P.A.M., 2006. Tectonothermal evolution of the northeastern margin of Iberia since the break-up of Pangea to present, revealed by low-temperature fission-track and (U-Th)/He thermochronology: A case history of the Catalan Coastal Ranges. Earth Planet Sci Lett 243, 159–180.

López-Geta, J.A., Baeza, J., Ramírez A., 2002. Las aguas minerales en España. Visión histórica, contexto hidrogeológico y persepectiva. Ministerio de Ciencia y Teconología.

Loveless, S., Pluymaekers, M., Lagrou, D., Boever, E. de, Doornenbal, H., Laenen, B., 2014. Mapping the geothermal potential of fault zones in the Belgium-Netherlands border region. Energy Procedia 59, 351–358. https://doi.org/10.1016/j.egypro.2014.10.388

Macau, A., Benjumea, B., Gabàs, A., Bellmunt, F., Figueras, S., 2018. Geophysical measurements for site effects characterisation in the urban area of Girona, Spain. Near Surface Geophysics 16, 340–355.

Mansfield, C., Cartwright, J., 2001. Fault growth by linkage: Observations and implications from analogue models. J Struct Geol 23, 745–763. https://doi.org/10.1016/S0191-8141(00)00134-6

Manzocchi, T., Heath, A.E., Palananthakumar, B., Childs, C., Walsh, J.J., 2008. Faults in conventional flow simulation models: A consideration of representational assumptions and geological uncertainties. Petroleum Geoscience 14, 91–110. https://doi.org/10.1144/1354-079306-775

Marcén, M., Casas-Sainz, A.M., Román-Berdiel, T., Griera, A., Santanach, P., Pocoví, A., Gil-Imaz, A., Aldega, L., Izquierdo-Llavall, E., 2018. Multiple movements recorded in a crustal weakness zone in NE Iberia: The Vallès-Penedès Fault revisited. J Geodyn 121, 96–114. https://doi.org/10.1016/j.jog.2018.07.003

Martín-Martín, M., Guerrera, F., Tosquella, J., Tramontana, M., 2021. Middle Eocene carbonate platforms of the westernmost Tethys. Sediment Geol 415, 105861. https://doi.org/10.1016/j.sedgeo.2021.105861

Mattsson, T., Burchardt, S., Mair, K., Place, J., 2020. Host-rock deformation during the emplacement of the Mourne Mountains granite pluton: Insights from the regional fracture pattern. Geosphere 16, 182–209. https://doi.org/10.1130/GES02148.1

Micklethwaite, A., Ford, A., Witt, W., Sheldon, A., 2014. The where and how of faults, fluids and permeability – insights from fault stepovers, scaling properties and gold mineralization. Geofluids, 15 (1-2), 240-251. https://doi.org/10.1111/gfl.12102

Mitjanas, G., Ledo, J., Macau, A., Alías, G., Queralt, P., Bellmunt, F., Rivero, L., Gabàs, A., Marcuello, A., Benjumea, B., Martí, A., Figueras, S., 2021. Integrated seismic ambient noise, magnetotellurics and gravity data for the 2D interpretation of the Vallès basin structure in the geothermal system of La Garriga-Samalús (NE Spain). Geothermics 93. https://doi.org/10.1016/j.geothermics.2021.102067

Nakamura, Y., 1989. A method for dynamic characteristics estimations of subsurface using microtremors on the ground surface. Railway Technical Research Institute, Quaterly Reports 30, 25–33.

Park, H.J., West, T.R., 2002. Sampling bias of discontinuity orientation caused by linear sampling technique. Eng Geol 66, 99–110. https://doi.org/10.1016/S0013-7952(02)00034-0

Passchier, C.W., Trouw, R.A.J., 2005. Microtectonics, 2nd Editio. ed.

Peacock, D.C.P., Sanderson, D.J., 1994. Geometry and development of relay ramps in normal fault systems. American Association of Petroleum Geologists Bulletin 78, 147–165. https://doi.org/10.1306/bdff9046-1718-11d7-8645000102c1865d

Price, N.J., Cosgrove, J.W., 1989. Analysis ot geological structures. Cambridge University Press.

Priest, S.D., 1993. Discontinuity Analysis for Rock Engineering. Chapman & Hall, London, UK.

Priest, S.D., Hudson, J.A., 1981. Estimation of discontinuity spacing and trace length using scanline surveys. International Journal of Rock Mechanics and Mining Sciences and 18, 183–197. https://doi.org/10.1016/0148-9062(81)90973-6

Rhén, I., Thunehed, H., Triumf, C.A., Follin, S., Hartley, L., Hermansson, J., Wahlgren, C.H., 2007. Development of a hydrogeological model description of intrusive rock at different investigation scales: An example from south-eastern Sweden. Hydrogeol J 15, 47–69. https://doi.org/10.1007/s10040-006-0124-2

Roca, E., 2001. The Northwest Mediterranean Basin (Valencia Trough, Gulf of Lions and Liguro-Provençal basins): structure and geodynamic evolution, in: Ziegler, P.A., Cavazza, W., Roberson, A.H.F., Crasquin-Soleau, S. (Eds.), Peri-Tethys Memoir 6: Peri-Tethyan Rift / Wrench Basins and Passive Margins. Memoires Du Museum National D’Histoire Naturelle, pp. 671–706.

Roca, E., 1996. La evolucion geodinamica de la Cuenca Catalano-Balear y areas adyacentes desde el Mesozoico hasta la actualidad. Acta Geologica Hispanica 29, 3–25.

Roca, E., 1992. L’estructura de la conca Catalano-Balear: paper de la compressiò i de la distensió en la seva gènesi. Universitat de Barcelona.

Roca, E., Guimerà, J., 1992. The Neogene structure of the eastern Iberian margin: Structural constraints on the crustal evolution of the Valencia trough (western Mediterranean). Tectonophysics 203, 203–218.

Roca, E., Sans, M., Cabrera, L., Marzo, M., 1999a. Oligocene to Middle Miocene evolution of the central Catalan margin (northwestern Mediterranean). Tectonophysics 315, 209–229.

Roca, E., Sans, M., Cabrera, L., Marzo, M., 1999b. Oligocene to Middle Miocene evolution of the central Catalan margin (northwestern Mediterranean). Tectonophysics 315, 209–229.

Rotevatn, A., Buckley, S.J., Howell, J.A., Fossen, H., 2009a. Overlapping faults and their effect on fluid flow in different reservoir types: A LIDAR-based outcrop modeling and flow simulation study. Am Assoc Pet Geol Bull 93, 407–427. https://doi.org/10.1306/09300807092

Rotevatn, A., Tveranger, J., Howell, J.A., Fossen, H., 2009b. Dynamic investigation of the effect of a relay ramp on simulated fluid flow: Geocellular modelling of the Delicate Arch Ramp, Utah. Petroleum Geoscience 15, 45–58. https://doi.org/10.1144/1354-079309-779

Sàbat, F., Roca, E., Muñoz, J.A., Vergés, J., Santanach, P., Sans, M., Masana, E., Estévez, A., Santisteban, C., 1995. Role of extension and compression in the evolution of the eastern margin of Iberia: the ESCI-València Trough seismic profile. Rev. Soc. Geol. España 8, 431–448.

Santanach, P., Casas, J.M., Gratacós, O., Liesa, M., Muñoz, J.A., Sàbat, F., 2011. Variscan and Alpine structure of the hills of Barcelona: geology in an urban area. Journal of Iberian Geology 37, 121–137.

Schön, J.H., 2015. Physical properties of rocks. Fundamentals and principles of petrophysics., 2nd ed. Developments in Petroleum Science.

Siebenaller, L., Boiron, M.C., Vanderhaeghe, O., Hibsch, C., Jessell, M.W., Andre-Mayer, A.S., France-Lanord, C., Photiades, A., 2013. Fluid record of rock exhumation across the brittle-ductile transition during formation of a Metamorphic Core Complex (Naxos Island, Cyclades, Greece). Journal of Metamorphic Geology 31, 313–338. https://doi.org/10.1111/jmg.12023

Siler, D.L., Hinz, N.H., Faulds, J.E., 2018. Stress concentrations at structural discontinuities in active fault zones in the western United States: Implications for permeability and fluid flow in geothermal fields. Bulletin of the Geological Society of America 130, 1273–1288. https://doi.org/10.1130/B31729.1

Süer, S., Güleç, N., Mutlu, H., Hilton, D.R., Çifter, C., Sayin, M., 2008. Geochemical monitoring of geothermal waters (2002-2004) along the North Anatolian fault zone, Turkey: Spatial and temporal variations and relationship to seismic activity. Pure Appl Geophys 165, 17–43. https://doi.org/10.1007/s00024-007-0294-4

Velde, B., Meunier, A., 2008. The Origin of Clay Minerals in Soils and Weathered Rocks. Springer Berlin Heidelberg, Berlin, Heidelberg. https://doi.org/10.1007/978-3-540-75634-7

Vidal, N., Gallart, J., Danobeitia, J.J., 1995. Contribution of the ESCI-Valéncia Trough Wide-Angle Data to a Crustal Transect in the NE Iberian Margin. Revista de la Sociedad Geologica de Espana.

Walsh, J.J., Torremans, K., Güven, J., Kyne, R., Conneally, J., Bonson, C., 2018. Fault-Controlled Fluid Flow Within Extensional Basins and Its Implications for Sedimentary Rock-Hosted Mineral Deposits. Society of Economic Geologists Special Publications 237–269. https://doi.org/10.5382/sp.21.11

Watkins, H., Bond, C.E., Healy, D., Butler, R.W.H., 2015. Appraisal of fracture sampling methods and a new workflow tocharacterise heterogeneous fracture networks at outcrop. J Struct Geol 72, 67–82. https://doi.org/10.1016/j.jsg.2015.02.001